J. Mech. Phys. Solids 201 (2025) 106163

Contents lists available at ScienceDirect

Journal of the Mechanics and Physics of Solids

journal homepage: www.elsevier.com/locate/jmps

Universal pull-off force for separating a rigid sphere from a membrane

Wanying Zheng, Zhaohe Dai *

Department of Mechanics and Engineering Science, State Key Laboratory for Turbulence and Complex Systems, College of Engineering, Peking University, Beijing 100871, China

ARTICLE INFO

Keywords:
Pull-off force
Johnson–Kendall–Roberts theory
Soap films
Föppl membranes
Hyperelastic membranes

ABSTRACT

A pull-off force F_c is required to separate two objects in adhesive contact. For a rigid sphere on an elastic slab, the classic Johnson–Kendall–Roberts (JKR) theory predicts $F_c = \frac{3}{2}\pi\gamma R_s$, where γ represents the interface adhesion or toughness and R_s is the radius of the sphere. Here, we investigate an alternative, extreme scenario: the pull-off force required to detach a rigid, frictionless sphere from a thin membrane, a scenario observed in a wide range of nature and engineering systems, such as nanoparticles on cell membranes, atomic force microscopy probes on atomically thin 2D material sheets, and electronic devices on flexible films. We show that, within the JKR framework, the pull-off forces in axisymmetric soap films, linearly elastic membranes, and nonlinear hyperelastic membranes are all given by $F_c = \pi\gamma R_s$. This result is remarkable as it indicates that the pull-off force for membranes is independent of the material's constitutive law, size, pretension, and solid surface tension.

1. Introduction

Membranes or thin-film materials are ubiquitous in a range of nature and engineering systems from cells and tissues to adhesives and electronics (Freund and Suresh, 2004; Vella, 2019; Akinwande et al., 2017). In these systems, the act of detaching an object from a thin membrane is as common and significant as establishing contact with it (Bico et al., 2018; Style et al., 2017; Paulsen, 2019). Relevant examples permeate various fields: In daily life, we might try to detach our finger from a bandage to perceive its stickiness. In architecture, the pulling of a sphere across a soap film has inspired lightweight structural designs, such as the roofs for the iconic Munich Olympic Stadium (Otto, 2015; Goldsmith, 2016). In physics, the detachment of a probe from atomically thin two-dimensional materials has provided critical insights into van der Waals interactions (Akinwande et al., 2017; Dai et al., 2020). In biomechanics, measuring detaching forces has advanced the understanding of cell adhesion, including interactions with nanocarriers for cancer therapy (Yi et al., 2011; Hu et al., 2018; Krieg et al., 2019). Similarly, flexible electronics and micro/nano-electromechanical systems abound with examples where detachment plays a central role (Yuk et al., 2019; Kim et al., 2012).

An important question underlying the diverse examples mentioned above is: *What governs the force required to detach a spherical object from thin membranes, commonly referred to as pull-off force?* For a sphere of radius R_s on a semi-infinite substrate, Bradley's model for rigid substrates gives the critical pull-off force as $F_c = 2\pi\gamma R_s$ (Bradley, 1932), while the Johnson–Kendall–Roberts (JKR) theory predicts $F_c = \frac{3}{2}\pi\gamma R_s$ for compliant substrates (Johnson et al., 1971), where γ is the interface adhesion energy or toughness. This apparent discrepancy has been reconciled by the Tabor parameter (Barber, 2018; Ciavarella et al., 2019). Remarkably, it has been shown that the JKR pull-off force remains unchanged for pre-stretched neo-Hookean half spaces (He and Ding, 2009; Yang,

* Corresponding author.
E-mail address: daizh@pku.edu.cn (Z. Dai).

https://doi.org/10.1016/j.jmps.2025.106163
Received 6 January 2025; Received in revised form 20 April 2025; Accepted 20 April 2025
Available online 3 May 2025

2011). Barber (2013) further proved that the JRK pull-off force is independent of the elastic modulus and the Bradley force is independent of intermolecular force law as long as the probe profile takes a quadratic form. In contrast, systems such as soap films, 2D materials, and polymeric sheets suggest a different, extreme regime—namely, the interaction of spheres with ultrathin membranes, where material and geometrical nonlinearities introduce significant complexities.

Indeed, the adhesive contact mechanics of highly bendable membranes have been studied from a number of perspectives. A particularly well-explored scenario, both theoretically and experimentally, involves pressurized or inflated films and membranes in adhesive contact with rigid flat surfaces (Williams, 1997; Plaut et al., 2003; Shi et al., 2011; Zhu et al., 2017, 2018; Dai et al., 2022; Fang et al., 2022; Chen and Dai, 2023) and Winkler-type deformable flat surfaces (Patil et al., 2014, 2015). The framework considering both large deformations and nonlinear material behaviors has also been systematically investigated (Long et al., 2010; Long and Hui, 2012; Srivastava and Hui, 2013; Laprade et al., 2013; Rao et al., 2021). However, in the context of membranes in adhesive contact with spheres or curved surfaces, the current understanding of the corresponding pull-off forces remains limited and, sometimes, inconsistent, primarily due to the use of *ad hoc* assumptions.

Shanahan (2000) first studied this problem by assuming constant membrane tension and approximating the sphere's shape as a paraboloid. Borodich and Galanov (2016) followed the same assumption and approximation and further explicitly derived $F_c = \pi\gamma R_s$. Ru (2020) demonstrated that this relationship holds for the adhesion of an elastic sphere to a constant-tension membrane. Using the same assumptions (i.e., constant membrane tension), Yuan and Wang (2021) have also recently obtained this result and demonstrated its weak dependence on membrane size (Yuan et al., 2024). However, Argatov (2021) employed the precise shape of the sphere and showed that $F_c = \pi\gamma R_s$ is invalid when the constant tension is small. Yang et al. (2023) further provided an analytical demonstration that the pull-off force can be tuned by applying transverse pressure to neo-Hookean membranes. In contrast, Yu et al. (2025) reported that under small pretension or small transverse pressure, a Hookean membrane always yields $F_c = \pi\gamma R_s$ under the assumption of a paraboloidal shape for the sphere.

This work aims to establish via formal variational analysis that the critical pull-off force for detaching a rigid sphere from a circular thin membrane is universally given by

$$F_c = \pi\gamma R_s,$$

using the concept of JKR adhesion and Griffith fracture. This force is irrespective of the material's constitutive behavior, membrane size, or pretension. We demonstrate this intriguing result using three representative systems: soap films (characterized by liquid surface tension), Föppl membranes (described by Hooke's material law and moderate-rotation geometry), and hyperelastic membranes (featuring nonlinear material laws and fully nonlinear geometry) with and without solid surface tension. The rest of the paper is organized as follows. In Section 2, we analyze the pull-off force for soap films, representing a simple material law combined with nonlinear geometry. In Section 3, we discuss the detachment of a sphere from a Föppl membrane, emphasizing the need for the consistent consideration of the geometrical nonlinearity in the membrane and the sphere. In Section 4, we address the coupled effects of geometric and material nonlinearities using hyperelastic membranes. In Section 5, we discuss the effect of constant solid surface tension on the pull-off behavior. Finally, we summarize the implications and limitations of this work in Section 6.

2. Soap films

We begin by discussing the detachment of a sphere from a soap film (Fig. 1), a phenomenon that has inspired the design of lightweight structures, as demonstrated in the tabletop experiments by Frei Otto and colleagues (Otto, 2015). Due to the low density and large surface area of soap films, surface tension plays a dominant role in the formation and equilibrium of the film. Specifically, for a soap film with a constant liquid surface tension γ_{sv}, the shape of the film can be described by the minimal-surface equation:

$$2\gamma_{sv}\left(\frac{1}{R_1}+\frac{1}{R_2}\right)=0, \tag{1}$$

where $1/R_1$ and $1/R_2$ represent the principal curvatures of the surface (Gennes et al., 2004). We illustrate the pull-off model in Fig. 1b, building on the snapshot of a soap film shown in Fig. 1a. Specifically, a circular soap film is fixed at $r = R_f$ and contacts a rigid sphere of radius R_s at $r = r_c$ with a contact angle θ_c. Note that the soap film behaves as if it has a hole in $r < r_c$.

The origin of the coordinate system is placed at the center of the undeformed film, and axisymmetry is exploited to express the principal curvatures in Eq. (1) as:

$$\frac{1}{R_1}=\frac{z''}{(1+z'^2)^{3/2}} \quad \text{and} \quad \frac{1}{R_2}=\frac{z'}{r(1+z'^2)^{1/2}}, \tag{2}$$

for $r_c \le r \le R_f$, where $z' = \mathrm{d}z/\mathrm{d}r$. Following Shanahan (2000), we integrate this second-order ordinary differential equation to obtain:

$$z = r_c \sin\theta\left[\cosh^{-1}\left(\frac{R_f}{|r_c\sin\theta|}\right)\mp\cosh^{-1}\left(\frac{r}{|r_c\sin\theta|}\right)\right], \tag{3}$$

for $r_c \le r \le R_f$. Note that $\mp$ here takes minus sign for θ_c below $\pi/2$. However, when the contact angle is between 90° and 180°, the film forms a back-to-back C shape (to be shown in Fig. 1e), i.e., that the function $z(r)$ has two values for $r \in (r_c\sin\theta, r_c)$, which can be described by Eq. (3). The boundary conditions applied to derive Eq. (3) are:

$$z'(r_c) = -\tan\theta \quad \text{and} \quad z(r_f) = 0, \tag{4}$$

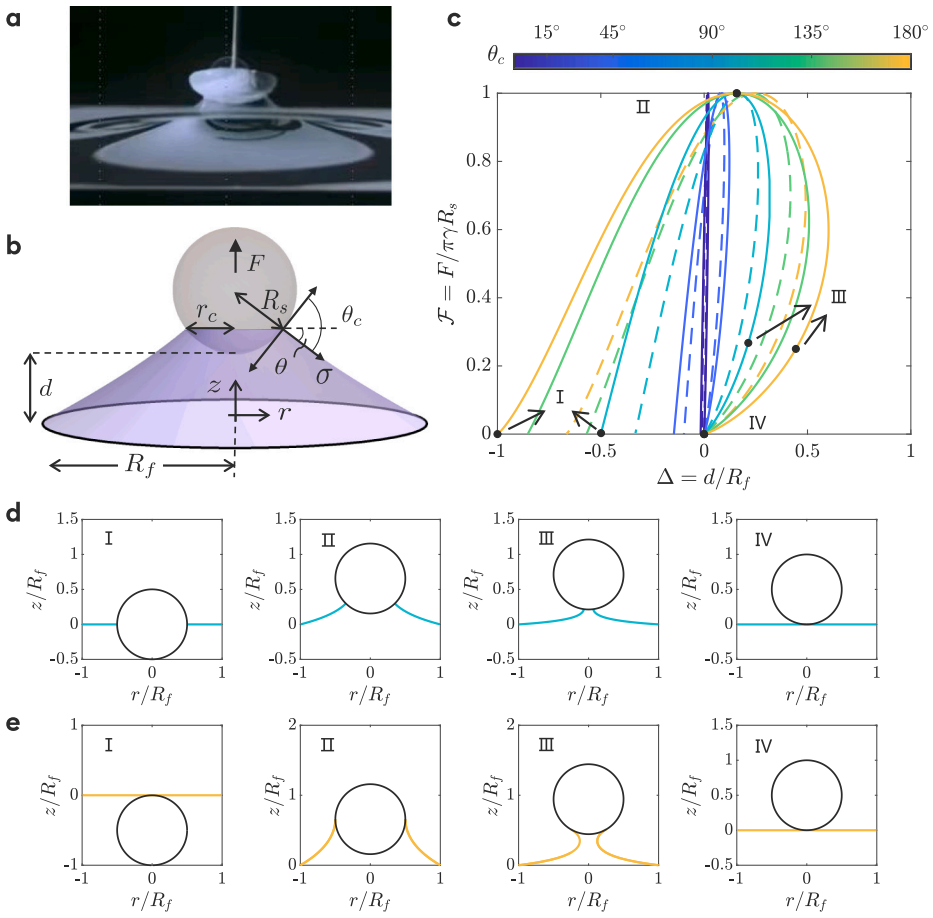

Fig. 1. Detachment from a freestanding soap film. (a) Photograph of a soap film at the moment of detachment (Otto, 2015). (b) Schematic illustration and notation for the detachment of a rigid sphere from the soap film under an applied pulling force. Here $\sigma = 2\gamma_{sv}$, where γ_{sv} is the surface tension of the liquid film. (c) Dimensionless pulling force–displacement relationships for various prescribed contact angles θ_c. Here $R_s = R_f/2$ for solid curves and $R_s = R_f/3$ for dashed curves. (d,e) Contours of the deformed soap film at different stages during detachment with $R_s = R_f/2$. $\theta_c = 90°$ in (d) and $\theta_c = 180°$ in (e). Note that there is no contact region in the theoretical setting, so the soap film in the contact region is not shown.

where θ is the clockwise-rotated angle of the film at the contact line (see Fig. 1b), satisfying the geometric relation:

$$z(r_c) = d + \left(R_s - \sqrt{R_s^2 - r_c^2}\right). \tag{5}$$

In theory, the soap film is allowed to move freely along the sphere's surface (Snoeijer and Andreotti, 2013). In practice, the contact angle typically relaxes to about $\pi/2$ in quasistatic experiments (see Fig. 1a). Without loss, we consider an arbitrary contact angle θ_c. The geometric relationship at the contact line implies

$$\theta = \theta_c - \arcsin\frac{r_c}{R_s}. \tag{6}$$

With these relations, for a given pulling displacement d, the shape of the deformed soap film can be determined, as well as the required pulling force:

$$F = 4\pi r_c \gamma_{sv} \sin\theta, \tag{7}$$

based on the vertical force balance at the contact line after making a circular cut at $r = r_c^+$. Finally, we define the "interface adhesion" along the line of the energy release rate in the peeling problem (Kendall, 1975; Freund and Suresh, 2004):

$$\gamma = \mathcal{G} = 2\gamma_{sv}(1 - \cos\theta_c). \tag{8}$$

Note that there is no true energy release rate for soap films since the interface crack is not well-defined. Another reason that we take the form of Eq. (8) is to make a consistent comparison with solid films of surface tension effect, to be discussed in Eq. (43).

In Fig. 1c, we present the calculated relationship between the rescaled pulling force and displacement based on Eqs. (3) to (8). For a fixed θ_c, two zero-force equilibrium states exist. Analogous to the soap-film catenoid, only the nontrivial branch (state I in

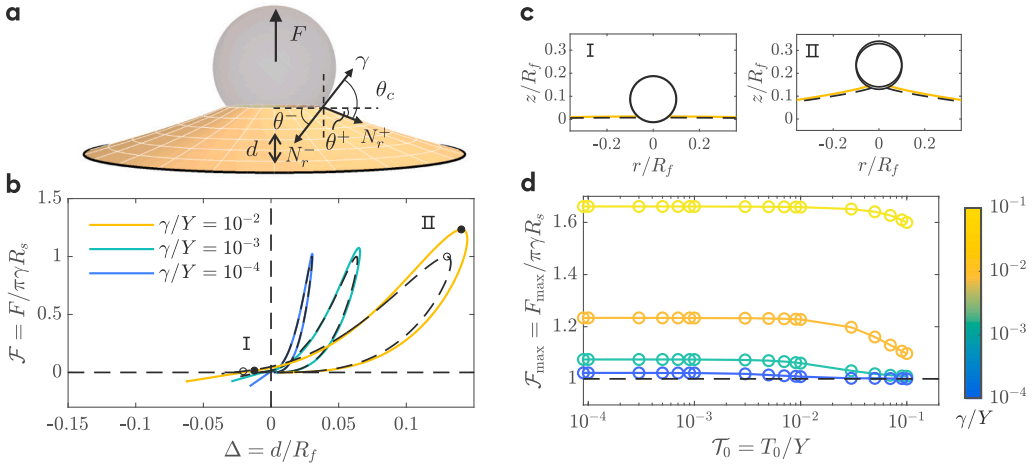

Fig. 2. Pull-off force of Föppl membranes. (a) Schematic illustration of an elastic membrane in adhesive contact with a rigid sphere under a pulling force. (b) Pulling force–displacement curves computed using the exact sphere shape (solid-colored curves) and the approximate sphere shape (i.e., paraboloid, dashed curves). The calculations consider three different interface adhesion values (see legend), a zero pretension (i.e., $\mathcal{T}_0 = T_0/Y = 0$), and a membrane size of $R_f/R_s = 10$. (c) Contours of membrane deformation at various stages of the pulling process (with $\gamma/Y = 10^{-2}$, $\mathcal{T}_0 = 0$, and $R_f/R_s = 10$). Here dashed curves used the parabolic approximation while solid curves used the exact shape of the sphere. (d) Influence of pretension and interface adhesion on the pull-off force of Föppl membranes. Note that the maximum pull-off force is unaffected by the specific membrane sizes in calculations using both the exact and approximate sphere shapes.

Fig. 1c) is stable (Israelachvili, 2011). Moreover, under force-controlled loading (pulling upward), the solution loses stability beyond state II (Barber, 2018).

A salient feature of these curves in Fig. 1 is the consistent maximum (or critical) pull-off force for various prescribed contact angles, θ_c, and sphere or film radii, R_s. This force is simply given by $F_c = \pi\gamma R_s$, even though the deformation behaviors differ. This result is not entirely new: It corresponds to twice the maximum pulling force of a sphere detaching from a liquid base (having only one side of the surface) where both gravity and capillarity are considered (Scheludko and Nikolov, 1975; Feng and Nguyen, 2017). Additionally, it matches the pull-off force observed when a sphere is detached from an elastic substrate with large surface tension or low modulus, under a linearized geometry approximation (Hui et al., 2015; Zhu et al., 2024). Fig. 1d and e illustrate the deformed configurations of the soap film at different pulling displacements for $\theta_c = 90°$ and $\theta_c = 180°$, respectively. It can be demonstrated that instabilities occur either after the maximum pulling force under force control or after the maximum pulling displacement under displacement control (Barber, 2018).

3. Föppl membranes

For soap films, the interface adhesion γ is defined by Eq. (8), which has enabled a unified pull-off force for any prescribed contact angle. In contrast, for elastic membranes, interface adhesion has a more physical interpretation, representing the energy required to propagate a crack at the sphere-film interface. Unlike soap films, membrane tension is not constant but depends instead on the specific material laws and residual stresses in the elastic membrane. Moreover, the contact angle θ_c is not prescribed but emerges as part of the solution to satisfy $\mathcal{G} = \gamma$, in line with Griffith fracture theory. Despite these fundamental differences, we will demonstrate that a comparable form of Eq. (8) exists for elastic membrane systems, leading to the same pull-off force $F_c = \pi\gamma R_s$, provided the nonlinear geometry of the film and the sphere is consistently accounted for.

We first consider pre-tensioned, linearly elastic membranes with moderate rotations, specifically Föppl membranes or the membrane limit of Föppl–von Kármán plates (Mansfield, 1989). This setup is valid when the aspect ratio of the deformed film—defined by both the ratio of overall deflection to the film radius and the ratio of downward deflection beneath the sphere to the sphere radius—is sufficiently large to render the bending effect negligible, yet small enough to avoid material nonlinearities (Dai and Lu, 2021). This condition is not particularly restrictive and can be easily satisfied in ultrathin membrane systems, such as polymeric films and 2D material sheets (Schroll et al., 2013; Yu et al., 2025). In this context, the radial and hoop strains can be related to the in-plane displacement $u(r)$ and the out-of-plane displacements $z(r)$ by

$$\epsilon_r = u' + \frac{1}{2}z'^2 \quad \text{and} \quad \epsilon_\theta = \frac{u}{r}, \tag{9}$$

which, together with Hooke's law, give radial and hoop stress resultants as

$$N_r = \frac{Y}{1-\nu^2}(\epsilon_r + \nu\epsilon_\theta) \quad \text{and} \quad N_\theta = \frac{Y}{1-\nu^2}(\epsilon_\theta + \nu\epsilon_r), \tag{10}$$

where Y and ν are the stretching stiffness and Poisson's ratio of the elastic membrane, respectively.

To calculate the energy release rate during the pulling process, we write the potential of the system with prescribed pulling displacement:

$$\Pi(u,u',z,z') = \int_0^{r_c} 2\pi r W(r,u,u')\,\mathrm{d}r + \int_{r_c}^{R_f} 2\pi r \left[W(r,u,u',z') - pz\right]\,\mathrm{d}r. \tag{11}$$

Here, p represents the external pressure (which is zero in this case) and the stretching energy densities of the membrane $W = \frac{1}{2}(N_r\epsilon_r + N_\theta\epsilon_\theta)$. As such, the energy release rate may be computed directly from the change in total potential energy per unit increase in cracked area. Importantly, this criterion is formally equivalent to minimizing the system's total free energy, $\mathcal{E} = \Pi$+total surface/interface, with the adhered area emerging as part of the solution. We therefore begin by applying the energy release method, which naturally recalls the classical peeling angle concepts of Kendall (1975) and Rivlin (1997).

Note that we have assumed a frictionless, adhesive sphere-membrane interface: the radial displacement of the membrane under the sphere is to be determined while the deflection of the membrane in the contact zone is given by the shape of the sphere:

$$z(r) = d + R_s - \sqrt{R_s^2 - r^2}, \tag{12}$$

for $r < r_c$. Under the condition of moderate rotation, this can be approximated as a parabola:

$$z(r) = d + \frac{r^2}{2R_s}. \tag{13}$$

Proceeding with the standard variation analysis under a non-pinning boundary condition (i.e., $\delta r_c \neq 0$) yields three Euler–Lagrange equations (see Appendix A), which can be rewritten as:

$$N_r\frac{\mathrm{d}^2 z}{\mathrm{d}r^2} + N_\theta\frac{1}{r}\frac{\mathrm{d}z}{\mathrm{d}r} = 0 \tag{14}$$

for $r_c < r < R_f$, and

$$N_\theta - \frac{\mathrm{d}}{\mathrm{d}r}(rN_r) = 0 \tag{15}$$

for $0 < r < R_f$. These equations represent the out-of-plane and in-plane equilibrium conditions of the membrane, respectively. Note that when the interfacial friction is considered, there will be an additional shear stress term in Eq. (15). The finite shear stress would likely remove the strain energy density term in the general form of the energy release rate (to be shown in Eq. (35)), as seen in the peeling problem reported by Begley et al. (2013) and explained via an alternative perspective by Ciavarella et al. (2023). We therefore speculate that the friction effect will modify the calculated pull-off force, but will not bring any Young's modulus dependence of the pull-off force. Precisely revealing such friction effect, however, is nontrivial, since it would depend on how the contact is established (i.e., the loading history) and detailed friction law (e.g., constant sliding stress used in Begley et al., 2013 vs. Coulomb law used in Barber and Stupkiewicz, 2024).

For numerical convenience, we use the Airy stress function φ such that Eq. (15) is satisfied automatically by calculating the radial and circumferential stress via $N_r = \varphi/r$ and $N_\theta = \mathrm{d}\varphi/\mathrm{d}r$. The problem is then to solve the out-of-plane equilibrium equation and compatibility equation in terms of φ and z (Mansfield, 1989):

$$\frac{\mathrm{d}}{\mathrm{d}r}\left(\varphi\frac{\mathrm{d}z}{\mathrm{d}r}\right) = 0 \quad \text{for} \quad r_c \le r \le R_f \quad \text{and} \quad r\frac{\mathrm{d}}{\mathrm{d}r}\left[\frac{1}{r}\frac{\mathrm{d}}{\mathrm{d}r}(r\varphi)\right] = -\frac{Y}{2}z'^2 \quad \text{for} \quad 0 \le r \le R_f. \tag{16}$$

This system of differential equations can be solved by combining the shape of the membrane in the contact region, as described in (12) or approximated in (13), along with the natural boundary conditions:

$$z'(0) = 0, \quad u(0) = \lim_{r\to 0} r\left[\varphi'(r) - \nu\frac{\varphi(r)}{r}\right] = 0, \quad z(R_f) = 0, \quad \varphi'(R_f) - \nu\frac{\varphi(R_f)}{R_f} = (1-\nu)T_0, \tag{17}$$

and physically informed matching conditions:

$$z(r_c^-) = z(r_c^+), \quad \varphi(r_c^-) = \varphi(r_c^+), \quad \varphi'(r_c^-) = \varphi'(r_c^+). \tag{18}$$

Here, T_0 represents the pretension in the clamped thin membrane so that the physical meaning of the last equation in Eq. (17) is that the membrane is clamped at its edge with a pre-stretched radial displacement $(1-\nu)T_0/Y$. It is important to note that Eq. (18) imposes the continuity of both radial and hoop stresses at the contact line. This requirement comes from the assumption of a frictionless interface (i.e., $u(r_c)$ is variable; see Appendix A), which is consistent with previous studies on similar problems such as wetting and blistering (Liu et al., 2020; Dai et al., 2022).

We then derive the energy release rate by assessing the change in total potential energy per unit area of newly formed surfaces or, conversely, contacted surfaces over sphere. Specifically,

$$\mathcal{G} = -\frac{\delta\Pi}{\delta A_{\text{fracture}}} = \frac{\delta\Pi}{\delta A_{\text{contact}}} = \frac{\delta\Pi}{2\pi r_c\delta r_c/\cos\theta^-}, \tag{19}$$

where θ^- denotes the inclination angle of the sphere or membrane at $r = r_c^-$ (see the notation in Fig. 2a). By combining this with the boundary term associated with δr_c from (A.19) in the variational analysis, we obtain:

$$\mathcal{G} = N_r^+(1-\cos\theta_c), \tag{20}$$

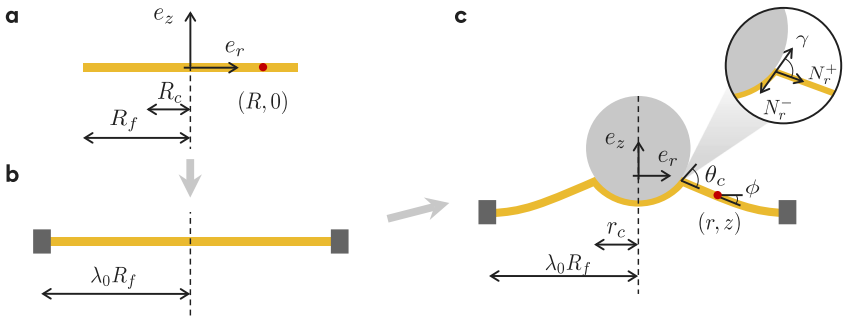

Fig. 3. Detachment of hyperelastic membrane: (a) the undeformed configuration, (b) the pre-stretched configuration, and (c) the final deformed configuration. In the inset illustrates the Young's relation at the contact.

where θ_c and N_r^+ are the contact angle and the membrane tension evaluated at $r = r_c^+$, respectively, as illustrated in Fig. 2a. Notably, this result for curved surfaces is identical to that for flat surfaces (Rao et al., 2021) and aligns with the concept of Kendall's thin-film peeling angle (Kendall, 1975; Thouless and Jensen, 1992; Hui et al., 2015). From geometry, we have $\theta_c = \theta^- + \theta^+$ and the inclination angle of the membrane at $r = r_c^+$ can be calculated by $\theta^+ = -\arctan z'(r_c^+)$ (Fig. 2a). It should be noted that for a spherical surface, $\theta^- = \arctan \frac{r_c}{\sqrt{R_s^2 - r_c^2}}$, as derived from (12); Under the parabolic approximation, Eq. (13) gives $\theta^- = \arctan(r_c/R_s)$. We limit ourselves by neglecting any mode-mixity (Hutchinson and Suo, 1991) so the energy required for the interface delamination can be characterized simply by adhesion energy between the sphere and the membrane γ, i.e.,

$$\mathcal{G} = \gamma. \tag{21}$$

The problem is fully defined by Eqs. (16) to (21), along with the spherical shape (12) or the approximated parabolic shape (13). We solve this multipoint boundary value problem numerically for a prescribed pulling displacement using MATLAB's BVP5C routine, incorporating a refined mesh near the contact line. Subsequently, the pulling force is determined based on the vertical force balance at the contact line:

$$F = 2\pi r_c N_r^+ \sin\theta^+. \tag{22}$$

Note that the contact pressure between the sphere and the elastic film does not come into play here since the cut is applied at $r = r_c^+$.

In Fig. 2b, we present the pulling force–displacement curves calculated using the exact (solid curves) and approximate (dashed curves) sphere shapes. Note that during the separating process, the solution after state II is unstable under the force-controlled loading. There are slight differences between the two, both in the pulling behavior and in the deformed geometry of the membrane (Fig. 2c). These differences become more pronounced with increasing adhesion, likely due to the larger contact area, which makes the approximated shape less valid. Interestingly, when the sphere shape is approximated by a paraboloid, the dimensionless critical pull-off force is consistently $\pi\gamma R_s$, regardless of the adhesion magnitude, membrane size, or pretension. In contrast, calculations using the exact sphere shape generally yield critical pull-off forces greater than $\pi\gamma R_s$. Furthermore, the difference from $\pi\gamma R_s$ decreases as the applied pretension T_0 increases or the adhesion decreases. This trend aligns with expectations, as large pretension and small adhesion correspond to smaller deformations of the membrane and also a smaller contact radius, by which the parabolic approximation of the sphere shape becomes more reasonable.

Despite such observations, we are not in a position to assert that calculations using the exact shape of the sphere are more accurate or that the pull-off force is not always given by $\pi\gamma R_s$. This is because the moderate-rotation assumption of the membrane limit of Föppl–von Kármán equations is not entirely consistent with the use of the exact sphere shape. In contrast, the parabolic approximation of the shape of the sphere aligns more naturally with the moderate rotation assumption (Mansfield, 1989; Audoly and Pomeau, 2000), resulting in $F_c = \pi\gamma R_s$ (see dashed curves in Fig. 2b and d). To resolve this inconsistency, we investigate the adhesive contact problem of hyperelastic membranes within the framework of large deformations, where the geometry can be treated in a consistent manner (Long et al., 2010).

4. Hyperelastic membranes

In this section, we consider hyperelastic membranes and distinguish the deformed membrane from its undeformed configuration. The cross-sectional view of the membrane before and after deformation is shown in Fig. 3. A circular, thin membrane with an initial radius of R_f and thickness t_0 is stretched equibiaxially to a radius of $\lambda_0 R_f$, after which it is clamped at its edge. Again, the sphere is in frictionless, adhesive contact with the stretched membrane and is pulled upward until separation.

The coordinate of a material point in the undeformed configuration can be specified as $(R, 0)$, which is displaced to the point $(r(R), z(R))$ in the deformed configuration. The three principal stretches along the radial, hoop, and thickness directions, respectively, are

$$\lambda_r = \sqrt{r'^2 + z'^2}, \quad \lambda_\theta = \frac{r}{R}, \quad \text{and} \quad \lambda_t = \frac{t}{t_0}, \tag{23}$$

where $()'$ represents $\mathrm{d}()/\mathrm{d}R$ in this section. We focus on incompressible materials, that is, $\lambda_r\lambda_\theta\lambda_t = 1$ so the thickness of the deformed membrane is $t = t_0/\lambda_r\lambda_\theta$. It is convenient to introduce $\phi(R)$ as the clockwise-rotated angle of the deformed membrane (r, z), which satisfies the following geometric relations:

$$\sin\phi = -\frac{z'}{\lambda_r}, \quad \cos\phi = \frac{r'}{\lambda_r}, \quad \text{and} \quad \tan\phi = -\frac{\mathrm{d}z}{\mathrm{d}r}. \tag{24}$$

The membrane tensions N_r and N_θ can be related to the strain energy density function, $W(\lambda_r, \lambda_\theta)$ by

$$N_r = t\sigma_r = \frac{t_0}{\lambda_\theta}\frac{\partial W}{\partial \lambda_r} \quad \text{and} \quad N_\theta = t\sigma_\theta = \frac{t_0}{\lambda_r}\frac{\partial W}{\partial \lambda_\theta}. \tag{25}$$

where σ_r and σ_θ are the radial and hoop Cauchy stress of the membrane, respectively. Clearly, the relation between membrane tensions and stretches of the hyperelastic membrane relies heavily on the constitutive law used. Here we adopt Gent material with strain-hardening behaviors (GenRivlint, 1996):

$$W = -\frac{\mu}{2}J_m \ln\left(1 - \frac{I_1 - 3}{J_m}\right), \tag{26}$$

where μ is the shear modulus, J_m is a material constant related to the limiting stretch of the membrane, and $I_1 = \lambda_r^2 + \lambda_\theta^2 + 1/(\lambda_r^2\lambda_\theta^2)$ is the first invariant of the left Cauchy–Green deformation tensor. We then have

$$N_r = \frac{-\mu t_0 J_m\left(\lambda_r^4\lambda_\theta^2 - 1\right)}{\lambda_r\lambda_\theta + \lambda_r^3\lambda_\theta^3\left(\lambda_r^2 + \lambda_\theta^2 - 3 - J_m\right)} \quad \text{and} \quad N_\theta = \frac{-\mu t_0 J_m\left(\lambda_r^2\lambda_\theta^4 - 1\right)}{\lambda_r\lambda_\theta + \lambda_r^3\lambda_\theta^3\left(\lambda_r^2 + \lambda_\theta^2 - 3 - J_m\right)}. \tag{27}$$

Note that as $J_m \gg 1$, the Gent model reduces to the neo-Hookean model: $W = \frac{\mu}{2}\left(\lambda_r^2 + \lambda_\theta^2 + 1/\lambda_r^2\lambda_\theta^2 - 3\right)$ (Rivlin, 1948). In this case, the membrane tensions simply read

$$N_r = \mu t_0\left(\lambda_r^4\lambda_\theta^2 - 1\right)/\left(\lambda_r^3\lambda_\theta^3\right) \quad \text{and} \quad N_\theta = \mu t_0\left(\lambda_r^2\lambda_\theta^4 - 1\right)/\left(\lambda_r^3\lambda_\theta^3\right). \tag{28}$$

We then examine the governing equation and energy release rate of the system. Here we express the total potential energy in a form slightly different from Eq. (11):

$$\Pi = 2\pi\int_0^{R_f} W(\lambda_r, \lambda_\theta)t_0 R\,\mathrm{d}R - 2\pi\int_0^{R_c} p\left[z - \left(d + R_s - \sqrt{R_s^2 - r^2}\right)\right] rr'\,\mathrm{d}R, \tag{29}$$

where p plays as a Lagrange multiplier to ensure the conformal contact of the membrane onto the sphere in the contact region and the size of the contact region R_c in the undeformed configuration are not known *a priori*. Using variational analysis similar to the preceding section, we can obtain the out-of-plane and in-plane equilibrium equations for hyperelastic membranes as

$$\frac{r'z'' - z'r''}{\left(r'^2 + z'^2\right)^{3/2}}N_r + \frac{z'}{r\left(r'^2 + z'^2\right)^{1/2}}N_\theta + p\mathcal{H}(R_c - R) = 0. \tag{30}$$

and

$$\frac{\mathrm{d}N_r}{\mathrm{d}R} + \frac{r'(N_r - N_\theta)}{r} = 0, \tag{31}$$

respectively, for $0 \le R \le R_f$, where $\mathcal{H}$ is the Heaviside step function, and the distribution of p is part of the solution, with which the shape of the membrane conforms to the sphere described by (12). So far, no constitutive relations have been employed to derive this pair of governing equations. We then use the membrane tension–stretch relations, as demonstrated in Eq. (27) for the Gent membranes and Eq. (28) for neo-Hookean membranes. It is worth noting that under the moderate-rotation assumptions, including $r' \to 1$ and $z'^2 \to 0$, Eqs. (30) and (31) reduce to Eqs. (14) and (15) for Föppl membranes. Furthermore, Eq. (30) is conceptually analogous to Eq. (1) for soap films, although the membrane tension and curvature are more complex due to the material law.

It is more convenient to solve this problem by reformulating Eqs. (30) and (31) into a set of ordinary differential equations (ODEs), as demonstrated previously by Long et al. (2010):

$$\begin{aligned}
\frac{\mathrm{d}\lambda_\theta}{\mathrm{d}R} &= \frac{\lambda_r\cos\phi - \lambda_\theta}{R},\\
\frac{\mathrm{d}z}{\mathrm{d}R} &= -\lambda_r\sin\phi,\\
\frac{\mathrm{d}\phi}{\mathrm{d}R} &= \frac{p\mathcal{H}(R_c - R)R\lambda_\theta\lambda_r - \lambda_r N_\theta\sin\phi}{R\lambda_\theta N_r},\\
\frac{\mathrm{d}\lambda_r}{\mathrm{d}R} &= \frac{\lambda_r(N_\theta - N_r)\cos\phi - \lambda_\theta(\partial N_r/\partial\lambda_\theta)(\lambda_r\cos\phi - \lambda_\theta)}{R\lambda_\theta(\partial N_r/\partial\lambda_r)},
\end{aligned} \tag{32}$$

Given the membrane shape within the contact region, i.e., Eq. (12), the problem can be solved using seven additional boundary and matching conditions (6 for the two-region ODEs and 1 for the unknown R_c). Naturally, we impose:

$$\lambda_r(0) = \lambda_\theta(0), \quad z(R_f) = 0, \quad \lambda_\theta(R_f) = \lambda_0, \tag{33}$$

where λ_0 represents the pre-stretch. Furthermore, we enforce the continuity conditions at the contact line:

$$z(r_c^-) = z(r_c^+), \quad \lambda_r(R_c^-) = \lambda_r(R_c^+), \quad \lambda_\theta(R_c^-) = \lambda_\theta(R_c^+). \tag{34}$$

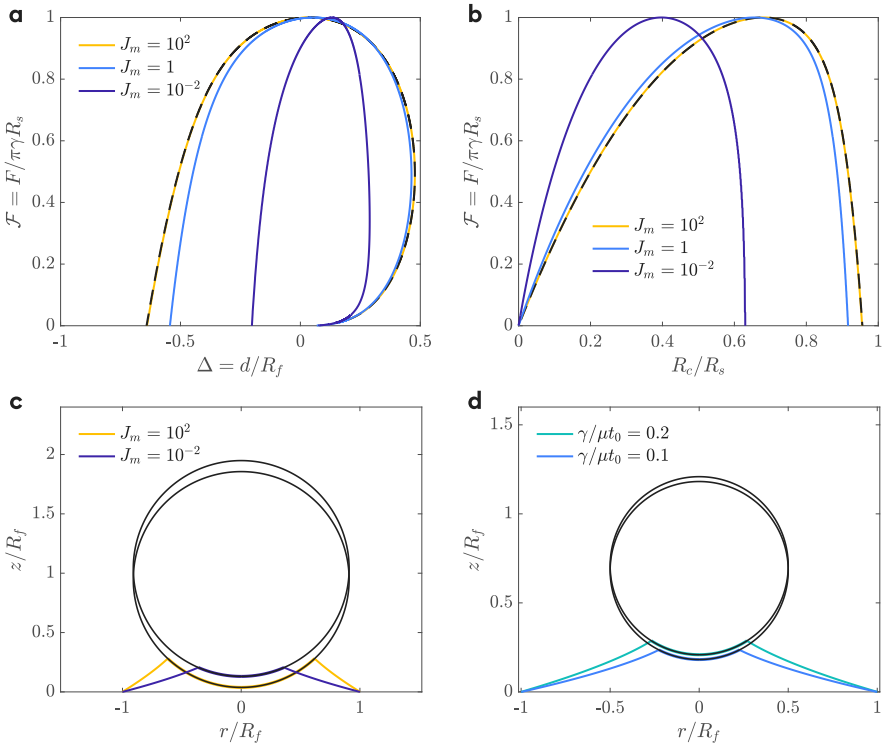

Fig. 4. Pull-off behavior of Gent hyperelastic membranes. (a) Pulling force–displacement curves calculated for membranes with different strain-stiffening behaviors (characterized by J_m as indicated in the legend). The dashed curve represents neo-Hookean membranes ($J_m \to \infty$). (b) Pulling force–contact radius relations for different material parameters. (c) The deformed contour of the membrane at the maximum pulling force for two different material parameters. In (a–c), we used adhesion energy $\gamma = 0.5\mu t_0$, the membrane size $R_f = 1.1R_s$, and a zero pre-stretching $\lambda_0 = 1$. (d) The deformed contour of the membrane at the maximum pulling force with two different adhesion energies. In this case, we used the membrane size $R_f = 2R_s$, the pre-stretching $\lambda_0 = 1$, and the material parameter $J_m = 500$.

Here, the continuity of λ_r across the contact line is a physical condition for frictionless interfaces. This setup differs from Long et al. (2010) and Yang et al. (2023), where λ_r is allowed to jump. However, this continuity is consistent with the variational analysis for Föppl membranes in the preceding section, as well as with relevant membrane problems involving lubricated interfaces. Examples include wetting on thin membranes in Liu et al. (2020), Andreotti and Snoeijer (2020), Rao et al. (2021) and blisters of atomically smooth 2D materials (Khestanova et al., 2016; Dai et al., 2018; Sanchez et al., 2018), where the continuity of strain components has been observed in Raman spectroscopy experiments (Kitt et al., 2013; Wang et al., 2017) and molecular dynamics simulations (Zhang and Arroyo, 2017; Yin et al., 2024).

Lastly, the no-pinning condition $\delta R_c \neq 0$ allows us to examine the increase in the total potential energy with the adhering area, leading to the energy release rate:

$$\mathcal{G} = \frac{\delta \Pi}{2\pi r_c \delta r_c / \cos\phi(R_c^-)} = N_r^+(1-\cos\theta_c) + \frac{t_0}{\lambda_r^- \lambda_\theta}\left[\frac{\partial W}{\partial \lambda_r}\Big|_{r=r_c^+}\Delta\lambda_r - \Delta W\right], \tag{35}$$

where $N_r^+ = N_r(R_c^+)$, $\theta_c = \phi(R_c^+) - \phi(R_c^-)$, $\Delta\lambda_r = \lambda_r^+ - \lambda_r^-$, $\Delta W = W(\lambda_r^+, \lambda_\theta) - W(\lambda_r^-, \lambda_\theta)$, and $\lambda_r^\pm$ are the radial stretches of the membrane evaluated at the outer and inner sides of the contact line. This result agrees with that obtained for flat surfaces by Long et al. (2010) and Rao et al. (2021). In addition, we note that applying $\lambda_r^- = 1$, Eq. (35) returns to the peeling of hyperelastic films given by Eremeyev and Naumenko (2015), which can be further transformed to Rivlin's formula (Rivlin, 1997) and Kendall's equation (Kendall, 1975). In the frictionless JKR framework, however, applying the continuity conditions given in Eq. (34) provides the last condition for determining the position of the contact line:

$$N_r^+(1-\cos\theta_c) = \gamma, \tag{36}$$

where θ_c again represents the local contact angle as illustrated in Fig. 3c. This result is similar to Eq. (8) for soap films and identical to Eq. (20) for Föppl membranes, though it holds for any thermodynamically allowable material law. A more intuitive understanding can be provided by the illustration in the inset of Fig. 3c, where θ_c can be considered as an elastic version of Young's angle.

We adopt a shooting method to solve the problem specified in Eqs. (32) to (36). The idea is to transform the multipoint boundary value problem into an initial value problem (see Appendix D for details). Given a material law, the pulling displacement d, and the effective adhesion $\Gamma = \gamma/\mu t_0$, we solve for the deformed configuration and the pulling force required to achieve the pulling

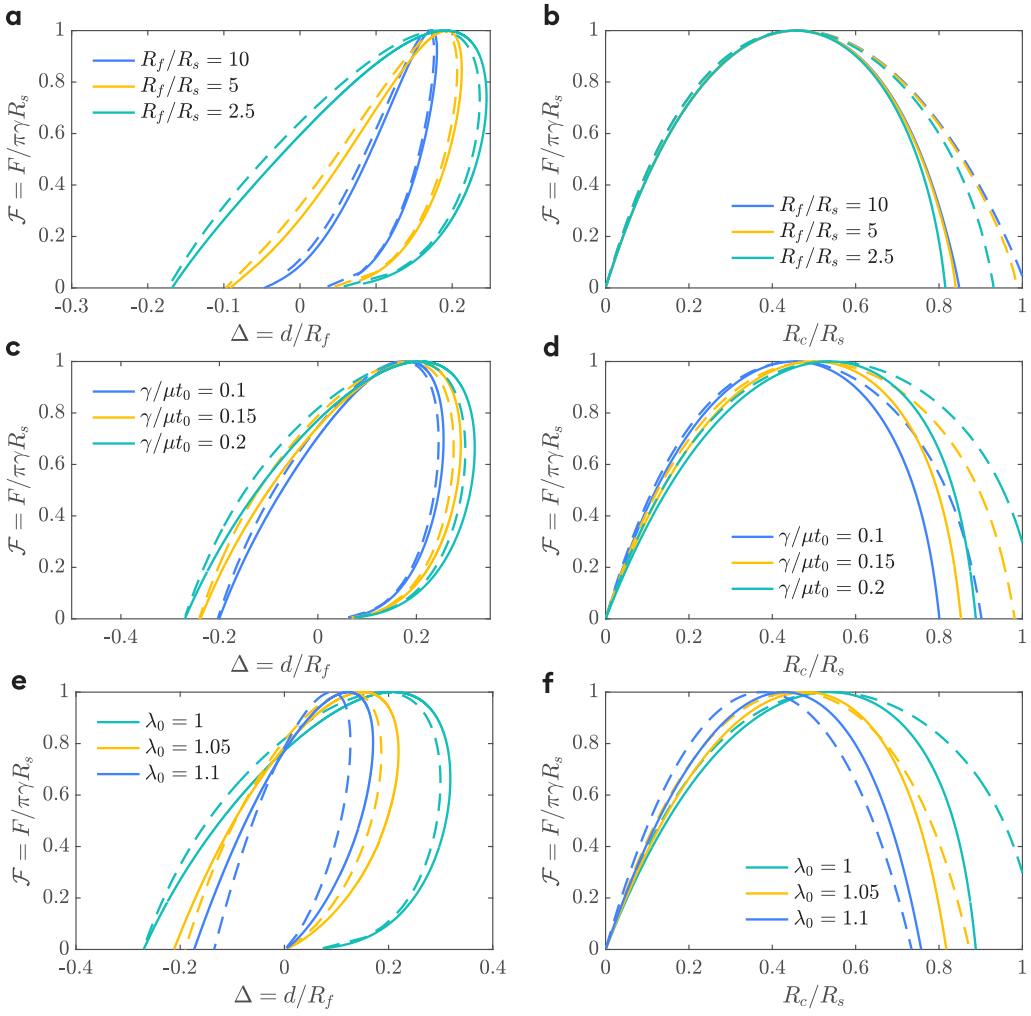

Fig. 5. Effect of membrane size, adhesion energy, and pre-stretch on the pull-off force. (a, b) Pulling force–displacement and pulling force–contact radius curves for various dimensionless membrane sizes. The adhesion energy is set to $\gamma/\mu t_0 = 0.1$, and the pre-stretch is zero. (c, d) Pulling force–displacement and pulling force–contact radius curves for various dimensionless adhesion energies, with $R_f/R_s = 2$ and zero pre-stretch. (e, f) Pulling force–displacement and pulling force–contact radius curves for various pre-stretch values, where $\gamma/\mu t_0 = 0.2$ and $R_f/R_s = 2$. All colored solid curves are calculated using a Gent hyperelastic membrane ($J_m = 500$) and the exact sphere shape. In contrast, all colored dashed curves are based on a linear Föppl membrane and a parabolic approximation for the sphere shape. Solid and dashed Curves with the same color are calculated using identical parameters, including membrane size, adhesion energy, and pre-stretch.

displacement, which is determined by the vertical force balance at the contact line:

$$F = 2\pi r_c N_r^+ \sin\phi(R_c^+). \tag{37}$$

Fig. 4a and b illustrate the influence of material laws on the pull-off behavior of the membrane. The calculations are based on $\gamma = \mu t_0/2$, $R_f = 1.1R_s$, zero pre-stretch ($\lambda_0 = 1$), and various J_m. As expected, the Gent membrane with a smaller J_m undergoes more restricted deformation due to its strain-stiffening behavior. For instance, the pulling force–contact radius curves in Fig. 4b show that membranes with smaller J_m generate smaller contact areas with the sphere. However, it may appear counterintuitive that the critical pulling displacement at which the pulling force reaches its maximum is not directly proportional to J_m (Fig. 4a). This phenomenon can be attributed to the geometry of the sphere, which influences the critical pulling displacement by the critical contact radius (Fig. 4c). Despite these nuances, somewhat surprisingly, the maximum pulling force for membranes with varying strain-stiffening behaviors is universally given by $F_c = \pi\gamma R_s$.

Fig. 5 illustrates the effects of other parameters, including membrane size, adhesion energy, and pre-stretch on the relation between the pulling force and pulling displacement as well as between the pulling force and the contact radius. We compare calculations for two systems: solid curves representing Gent hyperelastic membranes with the exact sphere shape and dashed curves representing linear Föppl membranes with the parabolic shape approximation, as discussed in the preceding section. For Föppl membranes, Young's modulus of the membrane is taken as $E = 3\mu$ (i.e., $\nu = 0.5$ for incompressibility).

Several noteworthy observations can be drawn from the results in Fig. 5. First, as expected, the difference between linear and nonlinear membrane behavior is minimal when the pulling displacement (and equivalently, the contact area) is small. Additionally, the pulling force–contact area relationship is relatively insensitive to membrane size, when $R_f \gtrsim R_s$ (Fig. 5b). Furthermore, the results in Fig. 5c–f indicate that the critical pulling displacement decreases as the dimensionless adhesion energy and pre-stretch decrease. Interestingly, in all cases, the maximum pulling forces (i.e., the pull-off forces) remain unchanged.

5. Effect of surface tension

Finally, we discuss the role of surface tension in the pull-off force for hyperelastic membranes. For simplicity, we consider constant surface tensions (Style et al., 2017; Bico et al., 2018). When surface tension is included, the energy release rate and adhesive toughness of the system are not immediately clear. We therefore write the total free energy of the system by incorporating the total potential energy in Eq. (29) along with the energy contributions from all surfaces and interfaces:

$$\mathcal{E} = \Pi + 4\pi R_s^2 \gamma_{sv} + \int_0^{r_c} 2\pi r(\gamma_{mv} + \gamma_{ms} - \gamma_{sv})\sqrt{r'^2 + z'^2}\,\mathrm{d}R + \int_{r_c}^{R_f} 2\pi r 2\gamma_{mv}\sqrt{r'^2 + z'^2}\,\mathrm{d}R, \tag{38}$$

where γ_{mv}, γ_{ms}, and γ_{sv} denote the surface energy densities of the membrane–vapor, membrane–sphere, and sphere–vapor interfaces, respectively. For notational convenience, we define a surface tension function:

$$T_s(R) = (\gamma_{mv} + \gamma_{ms} - \gamma_{sv})\mathcal{H}(R_c - R) + 2\gamma_{mv}\mathcal{H}(R - R_c). \tag{39}$$

Via a variational analysis detailed in Appendix C, we find that considering surface tension modifies the out-of-plane equilibrium Eq. (30) for the hyperelastic membrane as follows:

$$\frac{r'z'' - z'r''}{\left(r'^2 + z'^2\right)^{3/2}}(N_r + T_s) + \frac{z'}{r\left(r'^2 + z'^2\right)^{1/2}}(N_\theta + T_s) + p\mathcal{H}(R_c - R) = 0. \tag{40}$$

This result is consistent with the wetting problem reported by Liu et al. (2020) and the liquid blister problem in Rao et al. (2021), which conceptually represents a superposition of the elastic membrane Eq. (30) and the soap film Eq. (1). Consequently, the third equation in (32) must be rewritten as:

$$\frac{\mathrm{d}\phi}{\mathrm{d}R} = \frac{p\mathcal{H}(R_c - R)R\lambda_\theta\lambda_r - \lambda_r(N_\theta + T_s)\sin\phi}{R\lambda_\theta(N_r + T_s)}. \tag{41}$$

Note that under the assumption of constant surface tensions, the in-plane equilibrium Eq. (31) and the other equations in (32) remain unaffected.

When the equilibrium equations are satisfied, the minimization of total free energy (i.e., $\delta\mathcal{E} = 0$ with $\delta R_c \neq 0$) can be re-written as:

$$\begin{aligned} 0 &= \frac{\delta\mathcal{E}}{2\pi r_c \delta r_c / \cos\phi(R_c^-)} \\ &= \underbrace{\left(N_r^+ + 2\gamma_{mv}\right)(1 - \cos\theta_c) + \frac{t_0}{\lambda_r^-\lambda_\theta}\left[\frac{\partial W}{\partial \lambda_r}\Big|_{r=r_c^+}\Delta\lambda_r - \Delta W\right]}_{\text{Energy release rate: } \mathcal{G}} - \underbrace{(\gamma_{mv} + \gamma_{sv} - \gamma_{ms})}_{\text{Adhesive toughness: } \gamma} \end{aligned} \tag{42}$$

This suggests that we can still follow the conventional definition of interface adhesion, which is the energy required to create the membrane–vapor and sphere–vapor interfaces while removing the membrane–sphere interface per unit area. In addition, with $\Delta\lambda_r = \Delta W = 0$, $\mathcal{G} = \gamma$, Eq. (42) simplifies to

$$(N_r^+ + 2\gamma_{mv})(1 - \cos\theta_c) = \gamma, \tag{43}$$

which can again be interpreted as the force balance along the direction tangential to the sphere at the contact line (Fig. 3c). We should note that this simple form benefits from the assumption of constant surface tension: When the Shuttleworth effect is considered, $\Delta\lambda_r \neq 0$ and $\Delta W \neq 0$ in general (Liu et al., 2020; Andreotti and Snoeijer, 2020).

Again, we can employ the shooting method discussed in the preceding section and in Appendix D to solve the problem with the surface tension effect numerically. Now, the calculation of the pulling force needs to take the surface tension into account in the vertical force balance at the contact line:

$$F = 2\pi r_c(N_r^+ + 2\gamma_{mv})\sin\phi(R_c^+). \tag{44}$$

The numerical results are presented in Fig. 6. While surface tension exhibits a role similar to pre-stretch in stiffening the membrane, the pull-off force remains $\pi\gamma R_s$, regardless of whether a Föppl or hyperelastic membrane model is used.

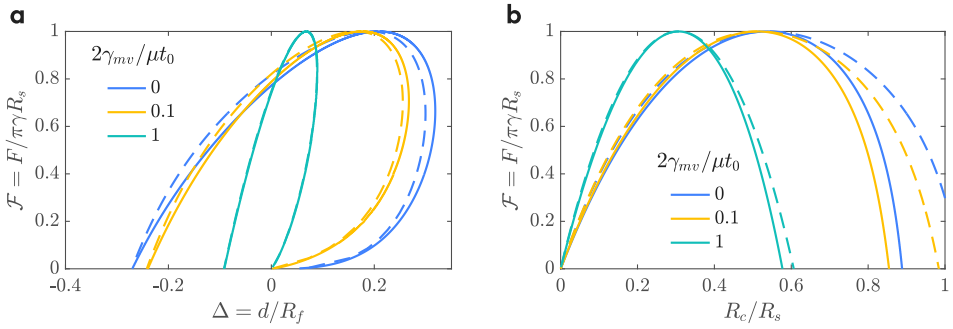

Fig. 6. Effect of surface tension on the detaching behavior. (a) Pulling force–displacement curves for various dimensionless surface tensions. Colored solid curves represent Gent hyperelastic membranes (with $J_m = 500$) while colored dashed curves represent Föppl membranes with the parabolic approximation for the sphere. Here we set $R_f = 2R_s$, $\gamma/\mu t_0 = 0.2$, and $\lambda_0 = 1$. (b) Pulling force–contact radius curves for various dimensionless surface tension.

6. Conclusions

We have investigated the force required to detach a sphere of radius R_s from a membrane. Our results demonstrate that as long as the energy release rate of the system is accurately accounted for and geometric nonlinearities are consistently considered, the pull-off force is universally given by $\pi\gamma R_s$, where γ represents the adhesion energy between the membrane and the sphere and R_s is the radius of the sphere. We have shown that this result is independent of the pretension or residual stress, the membrane size, and the specific material law through calculations with soap films, linearly elastic membranes, and hyperelastic membranes with and without surface tensions. This finding has potential applications in atomic force microscopy (AFM)-based measurements of 2D materials, polymeric films, and biological films such as cell membranes, particularly for interpreting the frequently observed finite pull-off forces (Krieg et al., 2019).

To reach the simple form of pull-off force described, we have made several important assumptions that warrant emphasis:

- Our analysis has been confined to axisymmetric configurations, whereas asymmetry may arise from various factors, including the geometry of the membrane, the geometry of the sphere, and the state of residual stress. When asymmetry is taken into account, the universal $F_c = \pi\gamma R_s$ may no longer hold, as suggested by previous studies on pull-off forces for anisotropically stretched elastic slabs (Zheng et al., 2019).
- Our current analysis has focused on nonlinear elastic membranes. However, for time-dependent systems, such as viscoelastic or poroelastic membranes (see discussion in Ciavarella et al., 2023), the fact that the pull-off force remains independent of Young's modulus suggests that $F_c = \pi\gamma R_s$ probably continues to hold.
- We assumed a frictionless interface between the sphere and the membrane. However, previous investigations into pressurized membranes with a no-slip interface (Yang et al., 2023) indicate that frictional effects at the interface could quantitatively alter the pull-off force.
- We neglected any mode-mixity effects in the interface delamination process. Such effects could play a significant role when pull-off occurs at large displacements, as discussed in earlier studies on similar blister problems (Hutchinson and Suo, 1991; Jensen and Thouless, 1993).
- We disregarded bending effects in the membrane and hence obtained jump in the membrane rotation across the contact (Li and Dai, 2024). In practice, bending effect is important within a boundary layer near the periphery of the contact line. The width of this boundary layer can be estimated as $(\mu t^3/N)^{1/2}$, where N represents the typical membrane tension (Davidovitch and Vella, 2018; Li et al., 2024). Therefore, this simplification is valid only when this length scale is much smaller than any horizontal scale in the system, including the sphere radius, membrane size, and contact radius.
- Our framework is based on the concept of JKR adhesion or Griffith fracture, which neglects the long-range nature of interface interactions. This assumption is reasonable only if the membrane is sufficiently compliant, according to the adhesion problem of half spaces (Ciavarella et al., 2019). For membranes of large modulus Y or subject to sufficiently large pretension T, we expect the transition to the Bradley limit, which has been partially discussed in Yu et al. (2025) for linearly elastic membranes via a membrane version of the Tabor parameter defined by $\gamma R_s/[z_0(T + \sqrt{\gamma Y})]$, where z_0 is some microscopic length.
- We did not consider the effect of any external pressure applied to the membrane, which can significantly alter the calculation of the pull-off force, as demonstrated in Yang et al. (2023).

In summary, the universal pull-off force reported here results from an extremely bendable thin membrane calculated within the concept of JKR adhesion and Griffith fracture. Nonetheless, we believe that addressing the subtleties mentioned above in future studies could provide deeper insights into the rich mechanics underlying the ubiquitous detachment phenomenon in thin membranes.

CRediT authorship contribution statement

Wanying Zheng: Writing – original draft, Methodology, Investigation, Formal analysis. **Zhaohe Dai:** Writing – review & editing, Validation, Supervision, Investigation, Funding acquisition, Formal analysis, Conceptualization.

Declaration of competing interest

The authors declare that they have no known competing financial interests or personal relationships that could have appeared to influence the work reported in this paper.

Acknowledgments

This work was financially supported by the National Natural Science Foundation of China (Grant No. 12372103 and 12432003).

Appendix A. Variational analysis of Föppl membranes

For Föppl membranes, we perform the variation on the total potential energy given in Eq. (11) with a movable contact radius (i.e., $\delta r_c \neq 0$):

$$\delta \Pi = 2\pi\delta \int_0^{r_c^-} \mathcal{F}_1 \,\mathrm{d}r + 2\pi\delta \int_{r_c^+}^{R_f} \mathcal{F}_2 \,\mathrm{d}r, \tag{A.1}$$

where

$$\mathcal{F}_1 = rW(r,u,u') \quad \text{and} \quad \mathcal{F}_2 = rW(r,u,u',z') - prz. \tag{A.2}$$

Specifically, based on the principle of variation, we have

$$\delta \int_0^{r_c^-} \mathcal{F}_1 \mathrm{d}r = \int_0^{r_c^-} \left(\frac{\partial \mathcal{F}_1}{\partial u}\delta u + \frac{\partial \mathcal{F}_1}{\partial u'}\delta u' \right) \mathrm{d}r + \mathcal{F}_1|_{r_c^-}\delta r_c^-, \tag{A.3}$$

where

$$\int_0^{r_c^-} \frac{\partial \mathcal{F}_1}{\partial u'}\delta u' \mathrm{d}r = \left.\frac{\partial \mathcal{F}_1}{\partial u'}\right|_{r_c^-} (\delta u)(r_c^-) - \left.\frac{\partial \mathcal{F}_1}{\partial u'}\right|_0 (\delta u)(0) - \int_0^{r_c^-} \frac{\mathrm{d}}{\mathrm{d}r}\left(\frac{\partial \mathcal{F}_1}{\partial u'}\right)\delta u \mathrm{d}r, \tag{A.4}$$

Note that the variation of the evaluation of a function $f(r)$ at the non-fixed boundary $r = r_c$ (i.e., $\delta f(r_c)$) could be different from the evaluation of the variation of this function, i.e., $(\delta f)(r_c)$. In particular, the two are related by

$$(\delta f)(r_c) = \delta f(r_c) - f'(r_c)\delta r_c. \tag{A.5}$$

The natural boundary conditions indicate the continuity of the position and the in-plane displacement at the contact line: $\delta r_c^- = \delta r_c^+ = \delta r_c$ and $\delta u(r_c^-) = \delta u(r_c^+) = \delta u_c$, where u_c is the in-plane displacement at the contact line. As a consequence, we obtain

$$\begin{aligned} &(\delta u)(r_c^-) = \delta u(r_c^-) - u'|_{r_c^-}\delta r_c^- = \delta u_c - u'|_{r_c^-}\delta r_c, \\ &(\delta u)(0) = \delta u(0) - u'|_0 \delta 0 = 0. \end{aligned} \tag{A.6}$$

Similarly, we proceed

$$\delta \int_{r_c^+}^{R_f} \mathcal{F}_2 \mathrm{d}r = \int_{r_c^+}^{R_f} \left(\frac{\partial \mathcal{F}_2}{\partial u}\delta u + \frac{\partial \mathcal{F}_2}{\partial u'}\delta u' + \frac{\partial \mathcal{F}_2}{\partial z}\delta z + \frac{\partial \mathcal{F}_2}{\partial z'}\delta z' \right) \mathrm{d}r + \mathcal{F}_2|_{R_f}\delta R_f - \mathcal{F}_2|_{r_c^+}\delta r_c^+, \tag{A.7}$$

where

$$\int_{r_c^+}^{R_f} \frac{\partial \mathcal{F}_2}{\partial u'}\delta u' \mathrm{d}r = \left.\frac{\partial \mathcal{F}_2}{\partial u'}\right|_{R_f} (\delta u)(R_f) - \left.\frac{\partial \mathcal{F}_2}{\partial u'}\right|_{r_c^+} (\delta u)(r_c^+) - \int_{r_c^+}^{R_f} \frac{\mathrm{d}}{\mathrm{d}r}\left(\frac{\partial \mathcal{F}_2}{\partial u'}\right)\delta u \,\mathrm{d}r \tag{A.8}$$

and

$$\int_{r_c^+}^{R_f} \frac{\partial \mathcal{F}_2}{\partial z'}\delta z' \mathrm{d}r = \left.\frac{\partial \mathcal{F}_2}{\partial z'}\right|_{R_f} (\delta z)(R_f) - \left.\frac{\partial \mathcal{F}_2}{\partial z'}\right|_{r_c^+} (\delta z)(r_c^+) - \int_{r_c^+}^{R_f} \frac{\mathrm{d}}{\mathrm{d}r}\left(\frac{\partial \mathcal{F}_2}{\partial z'}\right)\delta z \,\mathrm{d}r. \tag{A.9}$$

To simplify these results, we apply natural or physically informed boundary conditions:

$$\begin{aligned} &(\delta u)(R_f) = \delta u(R_f) - u'|_{R_f}\delta r_f = \delta u_f - u'|_{R_f}\delta R_f = 0, \\ &(\delta u)(r_c^+) = \delta u(r_c^+) - u'|_{r_c^+}\delta r_c^+ = \delta u_c - u'|_{r_c^+}\delta r_c, \\ &(\delta z)(R_f) = \delta z(R_f) - z'|_{R_f}\delta r_f = 0, \end{aligned} \tag{A.10}$$

and continuity condition of deflection at the contact line:

$$(\delta z)(r_c^+) = \delta z(r_c^+) - z'|_{r_c^+}\delta r_c^+ = \delta z_c - z'|_{r_c^+}\delta r_c. \tag{A.11}$$

Note that physically u_f in Eq. (A.10) is given by the pre-tensioned displacement (see Eq. (17) in the main text). Also note that since the deformed shape of the membrane (i.e., the relationship between r and z) in the contact region is known, δz_c in Eq. (A.11) can be calculated as

$$\delta z_c = z'|_{r_c^-}\delta r_c. \tag{A.12}$$

Based on these relations, the variation of the total potential energy can be rewritten as

$$\begin{aligned}\frac{\delta \Pi}{2\pi} = &\int_0^{r_c^-}\left[\frac{\partial \mathcal{F}_1}{\partial u} - \frac{\mathrm{d}}{\mathrm{d}r}\left(\frac{\partial \mathcal{F}_1}{\partial u'}\right)\right]\delta u\,\mathrm{d}r \\ &+\int_{r_c^+}^{R_f}\left\{\left[\frac{\partial \mathcal{F}_2}{\partial u} - \frac{\mathrm{d}}{\mathrm{d}r}\left(\frac{\partial \mathcal{F}_2}{\partial u'}\right)\right]\delta u + \left[\frac{\partial \mathcal{F}_2}{\partial z} - \frac{\mathrm{d}}{\mathrm{d}r}\left(\frac{\partial \mathcal{F}_2}{\partial z'}\right)\right]\delta z\right\}\mathrm{d}r \\ &+\left(\left.\frac{\partial \mathcal{F}_1}{\partial u'}\right|_{r_c^-} - \left.\frac{\partial \mathcal{F}_2}{\partial u'}\right|_{r_c^+}\right)\delta u_c \\ &+\left(\mathcal{F}_1|_{r_c^-} - \mathcal{F}_2|_{r_c^+} - \left.\frac{\partial \mathcal{F}_1}{\partial u'}u'\right|_{r_c^-} + \left.\frac{\partial \mathcal{F}_2}{\partial u'}u'\right|_{r_c^+} - \left.\frac{\partial \mathcal{F}_2}{\partial z'}z'\right|_{r_c^-} + \left.\frac{\partial \mathcal{F}_2}{\partial z'}z'\right|_{r_c^+}\right)\delta r_c.\end{aligned} \tag{A.13}$$

The variational terms of the displacement δu and δw can give rise to three Euler–Lagrange equations, which can be further specifically expressed as

$$\frac{\partial \mathcal{F}_1}{\partial u} - \frac{\mathrm{d}}{\mathrm{d}r}\left(\frac{\partial \mathcal{F}_1}{\partial u'}\right) = 0 \quad\Longrightarrow\quad N_\theta - \frac{\mathrm{d}}{\mathrm{d}r}(rN_r) = 0, \qquad 0 \le r < r_c, \tag{A.14}$$

$$\frac{\partial \mathcal{F}_2}{\partial u} - \frac{\mathrm{d}}{\mathrm{d}r}\left(\frac{\partial \mathcal{F}_2}{\partial u'}\right) = 0, \quad\Longrightarrow\quad N_\theta - \frac{\mathrm{d}}{\mathrm{d}r}(rN_r) = 0, \qquad r_c < r \le R_f, \tag{A.15}$$

and

$$\frac{\partial \mathcal{F}_2}{\partial z} - \frac{\mathrm{d}}{\mathrm{d}r}\left(\frac{\partial \mathcal{F}_2}{\partial z'}\right) = 0, \quad\Longrightarrow\quad N_r\frac{\mathrm{d}^2 z}{\mathrm{d}r^2} + N_\theta\frac{1}{r}\frac{\mathrm{d}z}{\mathrm{d}r} = p, \qquad r_c < r \le R_f. \tag{A.16}$$

The residual parts in Eq. (A.13) are considered as boundary terms. The variation of radial displacement at the contact line δu_c leads to

$$\left.\frac{\partial \mathcal{F}_1}{\partial u'}\right|_{r_c^-} - \left.\frac{\partial \mathcal{F}_2}{\partial u'}\right|_{r_c^+} = 0 \quad\Longrightarrow\quad N_r^- = N_r^+ \quad \text{at} \quad r = r_c, \tag{A.17}$$

where N_r^- and N_r^+ are the radial membrane tensions evaluated at the left (inner) and right (outer) side of the contact line, respectively. Therefore, this equation, together with the continuity of displacements, gives rise to the continuity of membrane tensions at the contact line. Lastly, the term associated with δc in Eq. (A.13) can be simplified:

$$-\left.\frac{\partial \mathcal{F}_1}{\partial u'}u'\right|_{r_c^-} + \mathcal{F}_1|_{r_c^-} + \left.\frac{\partial \mathcal{F}_2}{\partial u'}u'\right|_{r_c^+} - \left.\frac{\partial \mathcal{F}_2}{\partial z'}|_{r_c^+}z'\right|_{r_c^-} + \left.\frac{\partial \mathcal{F}_2}{\partial z'}z'\right|_{r_c^+} - \mathcal{F}_2|_{r_c^+} = \frac{N_r^+ r_c\left(1-\cos\theta_c\right)}{\cos\theta^-}, \tag{A.18}$$

at $r = r_c$. This means that when the equilibrium Eqs. (A.14) to (A.16) and the continuity condition (A.17) are satisfied and $\delta r_c \neq 0$, we end up with

$$\delta \Pi = 2\pi N_r^+(1-\cos\theta_c)r_c\delta r_c/\cos\theta^-, \tag{A.19}$$

which gives the energy release rate in Eq. (20) in the main text.

Appendix B. Variational analysis of hyperelastic membranes

It is more convenient to rewrite the total potential energy of the hyperelastic membrane in adhesive, frictionless contact with a rigid sphere

$$\Pi = 2\pi\int_0^{R_c}\mathcal{F}_1\mathrm{d}R + 2\pi\int_{R_c}^{R_f}\mathcal{F}_2\mathrm{d}R, \tag{B.1}$$

where

$$\mathcal{F}_1 = t_0 RW(r, r', z') - p\left[z - \left(d + R_s - \sqrt{R_s^2 - r^2}\right)\right]rr' \quad\text{and}\quad \mathcal{F}_2 = t_0 RW(r, r', z'). \tag{B.2}$$

The steps to obtain the governing equations and the energy release rate of the system are quite similar to those used for Föppl membranes in Appendix A. Specifically, we perform

$$\delta\Pi = 2\pi\delta\int_0^{R_c^-}\mathcal{F}_1\mathrm{d}r + 2\pi\delta\int_{R_c^+}^{R_f}\mathcal{F}_2\mathrm{d}r. \tag{B.3}$$

In the contact region, we have

$$\delta\int_0^{R_c^-}\mathcal{F}_1\mathrm{d}r = \int_0^{R_c^-}\left(\frac{\partial \mathcal{F}_1}{\partial r}\delta r + \frac{\partial \mathcal{F}_1}{\partial r'}\delta r' + \frac{\partial \mathcal{F}_1}{\partial z}\delta z + \frac{\partial \mathcal{F}_1}{\partial z'}\delta z'\right)\mathrm{d}R + \mathcal{F}_1\Big|_{R_c^-}, \tag{B.4}$$

where

$$\begin{aligned}\int_0^{R_c^-}\frac{\partial \mathcal{F}_1}{\partial r'}\delta r'\mathrm{d}r &= \left.\frac{\partial \mathcal{F}_1}{\partial r'}\right|_{R_c^-}(\delta r)(R_c^-)-\left.\frac{\partial \mathcal{F}_1}{\partial r'}\right|_{0}(\delta r)(0)-\int_0^{R_c^-}\frac{\mathrm{d}}{\mathrm{d}R}\left(\frac{\partial \mathcal{F}_1}{\partial r'}\right)\delta r\mathrm{d}R,\\ \int_0^{R_c^-}\frac{\partial \mathcal{F}_1}{\partial z'}\delta z'\mathrm{d}r &= \left.\frac{\partial \mathcal{F}_1}{\partial z'}\right|_{R_c^-}(\delta r)(R_c^-)-\left.\frac{\partial \mathcal{F}_1}{\partial z'}\right|_{0}(\delta r)(0)-\int_0^{R_c^-}\frac{\mathrm{d}}{\mathrm{d}R}\left(\frac{\partial \mathcal{F}_1}{\partial z'}\right)\delta z\mathrm{d}R.\end{aligned} \tag{B.5}$$

And in the non-contact region, we have

$$\delta\int_{R_c^+}^{R_f}\mathcal{F}_2\mathrm{d}r=\int_{R_c^+}^{R_f}\left(\frac{\partial \mathcal{F}_2}{\partial r}\delta r+\frac{\partial \mathcal{F}_2}{\partial r'}\delta r'+\frac{\partial \mathcal{F}_2}{\partial z}\delta z+\frac{\partial \mathcal{F}_2}{\partial z'}\delta z'\right)\mathrm{d}R+\mathcal{F}_2\Big|_{R_f}-\mathcal{F}_2\Big|_{R_c^+}, \tag{B.6}$$

where

$$\begin{aligned}\int_{R_c^+}^{R_f}\frac{\partial \mathcal{F}_2}{\partial r'}\delta r'\mathrm{d}r &= \left.\frac{\partial \mathcal{F}_2}{\partial r'}\right|_{R_f}(\delta r)(R_f)-\left.\frac{\partial \mathcal{F}_2}{\partial r'}\right|_{R_c^+}(\delta r)(R_c^+)-\int_{R_c^+}^{R_f}\frac{\mathrm{d}}{\mathrm{d}R}\left(\frac{\partial \mathcal{F}_2}{\partial r'}\right)\delta r\mathrm{d}R,\\ \int_{R_c^+}^{R_f}\frac{\partial \mathcal{F}_2}{\partial z'}\delta z'\mathrm{d}r &= \left.\frac{\partial \mathcal{F}_2}{\partial z'}\right|_{R_f}(\delta r)(R_f)-\left.\frac{\partial \mathcal{F}_2}{\partial z'}\right|_{R_c^+}(\delta r)(R_c^+)-\int_{R_c^+}^{R_f}\frac{\mathrm{d}}{\mathrm{d}R}\left(\frac{\partial \mathcal{F}_2}{\partial z'}\right)\delta z\mathrm{d}R.\end{aligned} \tag{B.7}$$

Plugging Eqs. (B.4)–(B.7) into (B.3) yields

$$\begin{aligned}\frac{\delta\Pi}{2\pi}=&\int_0^{R_c^-}\left[\left(\frac{\partial \mathcal{F}_1}{\partial r}-\frac{\mathrm{d}}{\mathrm{d}R}\frac{\partial \mathcal{F}_1}{\partial r'}\right)\delta r+\left(\frac{\partial \mathcal{F}_1}{\partial z}-\frac{\mathrm{d}}{\mathrm{d}R}\frac{\partial \mathcal{F}_1}{\partial z'}\right)\delta z\right]\mathrm{d}R\\ &+\int_{R_c+}^{R_f}\left[\left(\frac{\partial \mathcal{F}_2}{\partial r}-\frac{\mathrm{d}}{\mathrm{d}R}\frac{\partial \mathcal{F}_2}{\partial r'}\right)\delta r+\left(\frac{\partial \mathcal{F}_2}{\partial z}-\frac{\mathrm{d}}{\mathrm{d}R}\frac{\partial \mathcal{F}_2}{\partial z'}\right)\delta z\right]\mathrm{d}R\\ &-\left.\frac{\partial \mathcal{F}_1}{\partial r'}\right|_0(\delta r)(0)-\left.\frac{\partial \mathcal{F}_1}{\partial z'}\right|_0(\delta z)(0)\\ &+\mathcal{F}_1|_{R_c^-}\delta R_c^-+\left.\frac{\partial \mathcal{F}_1}{\partial r'}\right|_{R_c^-}(\delta r)(R_c^-)+\left.\frac{\partial \mathcal{F}_1}{\partial z'}\right|_{R_c^-}(\delta z)(R_c^-)\\ &-\mathcal{F}_2|_{R_c^+}\delta R_c^+-\left.\frac{\partial \mathcal{F}_2}{\partial r'}\right|_{R_c^+}(\delta r)(R_c^+)-\left.\frac{\partial \mathcal{F}_2}{\partial z'}\right|_{R_c^+}(\delta z)(R_c^+)\\ &+\mathcal{F}_2|_{R_f}\delta R_f+\left.\frac{\partial \mathcal{F}_2}{\partial r'}\right|_{R_f}(\delta r)(R_f)+\left.\frac{\partial \mathcal{F}_2}{\partial z'}\right|_{R_f}(\delta z)(R_f).\end{aligned} \tag{B.8}$$

For all arbitrary (r, z), the principle of virtual potential gives four Euler–Lagrange equations that can be combined as

$$p\mathcal{H}(R_c-R)=-\frac{t_0}{rz'}\left[\frac{\partial W}{\partial\lambda_\theta}-\frac{r'}{\lambda_r}\frac{\partial W}{\partial\lambda_r}-R\left(\frac{r'}{\lambda_r}\right)'\frac{\partial W}{\partial\lambda_r}-R\frac{r'}{\lambda_r}\left(\frac{\partial W}{\partial\lambda_r}\right)'\right] \tag{B.9}$$

and

$$p\mathcal{H}(R_c-R)=-\frac{t_0}{rr'}\left[\frac{z'}{\lambda_r}\frac{\partial W}{\partial\lambda_r}-R\left(\frac{z'}{\lambda_r}\right)'\frac{\partial W}{\partial\lambda_r}-R\frac{z'}{\lambda_r}\left(\frac{\partial W}{\partial\lambda_r}\right)'\right], \tag{B.10}$$

for $0\le R\le R_f$, where $\mathcal{H}$ is the Heaviside step function. To reach so, we have used the following relations

$$\frac{\partial W}{\partial r}=\frac{1}{R}\frac{\partial W}{\partial\lambda_\theta},\quad \frac{\partial W}{\partial r'}=\frac{r'}{\lambda_r}\frac{\partial W}{\partial\lambda_r},\quad \frac{\partial W}{\partial z}=0,\quad \frac{\partial W}{\partial z'}=\frac{z'}{\lambda_r}\frac{\partial W}{\partial\lambda_r}. \tag{B.11}$$

Combining potential energy integral functions (B.2), Euler–Lagrange equations, and these derivative relations we obtain the relationship

Plugging Eq. (25) into the sum of Eqs. (B.9) and (B.10) gives rise to the out-of-plane equilibrium Eq. (30) in the main text, which can be rewritten as

$$\kappa_r N_r+\kappa_\theta N_\theta+p\mathcal{H}(R_c-R)=0, \tag{B.12}$$

where κ_r and κ_θ denote the principal curvatures in the directions of the principal stretches λ_r and λ_θ, respectively. The geometric relationship requires

$$\kappa_r=-\frac{\mathrm{d}\phi}{\mathrm{d}\xi}=-\frac{\phi}{\lambda_r}\quad\text{and}\quad\kappa_\theta=-\frac{\sin\phi}{r}. \tag{B.13}$$

Similarly, plugging Eq. (25) into the difference between Eqs. (B.9) and (B.10) gives rise to the in-plane equilibrium Eq. (31) in the main text, which can be further rewritten as

$$\frac{\mathrm{d}N_r}{\mathrm{d}\lambda_\theta}\lambda_\theta'+\frac{\mathrm{d}N_r}{\mathrm{d}\lambda_r}\lambda_r'+\frac{r'(N_r-N_\theta)}{r}=0. \tag{B.14}$$

Combining Eqs. (B.12) to (B.14) and the definition of rotation angle in Eq. (24) leads to a set of first-order ordinary differential equations for $\{z,\phi,\lambda_r,\lambda_\theta\}$ for numerical convenience (Long et al., 2010; Rao et al., 2021), as shown in Eq. (32) in the main text.

Then we examine the energy release rate by considering the residual parts in Eq. (B.8). To proceed, we note that there exist

$$\frac{\partial \mathcal{F}_1}{\partial r'} = \frac{\partial W}{\partial r'} t_0 R = \frac{r'}{\lambda_r}\frac{\partial W}{\partial \lambda_r} t_0 R = \frac{r'}{\lambda_r}\frac{\lambda_\theta N_r}{t_0} t_0 R = \frac{r'}{\lambda_r} r N_r, \tag{B.15}$$

and

$$\frac{\partial \mathcal{F}_1}{\partial z'} = \frac{\partial W}{\partial z'} t_0 R = \frac{z'}{\lambda_r}\frac{\partial W}{\partial \lambda_r} t_0 R = \frac{z'}{\lambda_r}\frac{\lambda_\theta N_r}{t_0} t_0 R = \frac{z'}{\lambda_r} r N_r, \tag{B.16}$$

where we have used the condition of $\partial \Pi / \partial p = 0$ to cancel the term of p out. Note that $\partial \mathcal{F}_2 / \partial r'$ and $\partial \mathcal{F}_2 / \partial z'$ have the same calculation rule. In addition, the variational term at the contact line can be evaluated as

$$\begin{aligned} (\delta r)(R_c^{\pm}) &= \delta r(R_c^{\pm}) - r'|_{R_c^{\pm}} \delta R_c^{\pm} = \delta r_c - r'|_{R_c^{\pm}} \delta R_c, \\ (\delta z)(R_c^{\pm}) &= \delta z(R_c^{\pm}) - z'|_{R_c^{\pm}} \delta R_c^{\pm} = \delta z_c - z'|_{R_c^{\pm}} \delta R_c. \end{aligned} \tag{B.17}$$

Physically, we have the continuity of vertical displacement and hence

$$\delta z_c = \left(\frac{\partial z}{\partial r}\delta r\right)_{R_c^-} = \left.\frac{\mathrm{d}z}{\mathrm{d}r}\right|_{R_c^-} \delta r_c. \tag{B.18}$$

Combining equations Eqs. (B.15)–(B.18), (B.8) in equilibrium reads

$$\begin{aligned} \frac{\delta \Pi}{2\pi} = &\left[(-\lambda_r^- N_r^- + \lambda_r^+ N_r^+) r_c + t_0 R_c (W^- - W^+)\right] \delta R_c \\ &+ \left(\left.\frac{r r'}{\lambda_r}\right|_{R_c^-} N_r^- + \left.\frac{z'}{\lambda_r}\right|_{R_c^-} r_c N_r^- \left.\frac{\mathrm{d}z}{\mathrm{d}r}\right|_{R_c^-} - \left.\frac{r r'}{\lambda_r}\right|_{R_c^+} N_r^+ - \left.\frac{z'}{\lambda_r}\right|_{R_c^+} r_c N_r^+ \left.\frac{\mathrm{d}z}{\mathrm{d}r}\right|_{R_c^-} \right) \delta r_c. \end{aligned} \tag{B.19}$$

We exploit the geometric relationship (24), the hoop stretching $r_c = \lambda_\theta R_c$, and the calculus of variation $\delta r_c = r'^- \delta R_c$ to obtain

$$\frac{\delta \Pi}{2\pi} = \left[\left(\frac{\lambda_r^+}{\lambda_r^-} N_r^+ - \cos\theta_c N_r^+\right) + \frac{t_0}{\lambda_\theta \lambda_r^-}\left(W^- - W^+\right)\right] \frac{r_c}{\cos\phi^-} \delta r_c, \tag{B.20}$$

which gives rise to the energy release rate, i.e., Eq. (35) in the main text.

Appendix C. Hyperelastic membranes with surface tension

We demonstrate the energy variation for the hyperelastic membrane considering surface tension, emphasizing the differences with the derivation in Appendix B, where the surface tension is absent. Firstly, the integral function of total free energy reads

$$\begin{aligned} \mathcal{F}_1 &= t_0 R W(r, r', z') - p[z - (d + R_s - \sqrt{R_s^2 - r^2})] r r' + (\gamma_{mv} + \gamma_{ms} - \gamma_{sv}) r \sqrt{r'^2 + z'^2}, \\ \mathcal{F}_2 &= t_0 R W(r, r', z') + 2\gamma_{mv} r \sqrt{r'^2 + z'^2}. \end{aligned} \tag{C.1}$$

We can see that the variables in the surface energy section are only concerned with r, r', and z', thus the general form of variation does not change, i.e., Eqs. (B.4) to (B.7) are still valid. The detailed expressions in Eqs. (B.9) and (B.10) change to

$$\begin{cases} p\mathcal{H}(R_c - R) = -\dfrac{t_0}{r z'}\left[\dfrac{\partial W}{\partial \lambda_\theta} - \dfrac{r'}{\lambda_r}\dfrac{\partial W}{\partial \lambda_r} - R\left(\dfrac{r'}{\lambda_r}\right)'\dfrac{\partial W}{\partial \lambda_r} - R\dfrac{r'}{\lambda_r}\left(\dfrac{\partial W}{\partial \lambda_r}\right)'\right] - T_s(\kappa_r + \kappa_\theta), \\ p\mathcal{H}(R_c - R) = -\dfrac{t_0}{r r'}\left[\dfrac{z'}{\lambda_r}\dfrac{\partial W}{\partial \lambda_r} - R\left(\dfrac{z'}{\lambda_r}\right)'\dfrac{\partial W}{\partial \lambda_r} - R\dfrac{z'}{\lambda_r}\left(\dfrac{\partial W}{\partial \lambda_r}\right)'\right] - T_s(\kappa_r + \kappa_\theta), \end{cases} \tag{C.2}$$

where κ_r and κ_θ are given in Eq. (B.13). The out-of-plane equilibrium equation is obtained by computing the average between two equations in Eq. (C.2) while the in-plane is obtained by computing the difference between the two equations, thus the surface tension term (the last term) would appear in the out-of-plane equilibrium but not in the in-plane equilibrium. The boundary terms in the variation has been given in Eq. (42) in the main text.

Appendix D. Numerical scheme

We use the shooting method to numerically solve the set of differential equations discussed in Sections 4 and 5. For notation convenience, we first define dimensionless variables:

$$\{y_1, y_2, y_3, y_4\} = \{\lambda_\theta, z/R_f, \phi, \lambda_r\} \tag{D.1}$$

and

$$\mathcal{P} = pR_f \mathcal{H}(\widetilde{R}_c - \widetilde{R})/(\mu t_0), \quad \widetilde{R} = R/R_f, \quad \widetilde{R}_s = R_s/R_f \quad \text{and} \quad \mathcal{T}_s = T_s/\mu t_0. \tag{D.2}$$

Using Gent hyperelastic model (27), Eq. (32) with surface tension effect can be rewritten as

$$\begin{aligned}
&\frac{\mathrm{d}}{\mathrm{d}\widetilde{R}}y_1 = \frac{y_4\cos y_3 - y_1}{\widetilde{R}},\\
&\frac{\mathrm{d}}{\mathrm{d}\widetilde{R}}y_2 = -y_4\sin y_3,\\
&\frac{\mathrm{d}}{\mathrm{d}\widetilde{R}}y_3 = -\frac{y_4\sin y_3\left(y_4^2y_1^4 - 1 + \mathcal{T}_s y_4^3y_1^3\beta\right)/\widetilde{R} - \mathcal{P}y_4^4y_1^4\beta}{y_1\left(y_4^4y_1^2 - 1 + \mathcal{T}_s y_4^3y_1^3\delta\right)},\\
&\frac{\mathrm{d}}{\mathrm{d}\widetilde{R}}y_4 = \frac{\beta y_4^2\left(y_4^2y_1^4 - 3\right)\cos y_3 - \beta y_4y_1\left(y_4^4y_1^2 - 3\right)}{\widetilde{R}y_1\left[\left(y_4^4y_1^2+3\right)\beta + 2\left(y_4^4y_1^2-1\right)^2/(J_m y_4^2y_1^2)\right]} + \frac{2y_4\left(y_4^6y_1^6 - y_4^2y_1^2I_1 + 2\right)\left(-y_4\cos y_3 + y_1\right)}{\widetilde{R}y_1\left[y_4^2y_1^2\left(y_4^4y_1^2+3\right)J_m\beta + 2\left(y_4^4y_1^2-1\right)^2\right]},
\end{aligned} \tag{D.3}$$

where $\beta = 1-(I_1-3)/J_m$. In the contact region, the variables y_2 and y_3 can be directly obtained based on the shape of the sphere, specifically

$$y_2 = \Delta + \widetilde{R}_s - \sqrt{\widetilde{R}_s^2 - (y_1\widetilde{R})^2} \quad \text{and} \quad y_3 = -\arctan\widetilde{R}/\sqrt{\widetilde{R}_s^2 - (y_1\widetilde{R})^2}. \tag{D.4}$$

This boundary value problem can be readily solved via the shooting method. The contact region is solved by guessing a principal stretch, k, at $\widetilde{R} = \epsilon$ with $\epsilon \to 0$:

$$y_1(\epsilon) = k, \quad y_2(\epsilon) = \Delta, \quad y_3(\epsilon) = 0, \quad y_4(0) = k. \tag{D.5}$$

The non-contact region can then be solved using the four continuity/jump conditions at $\widetilde{R} = \widetilde{R}_c$ given in Eqs. (34) and (36) (for hyperelastic membranes without surface tension) or Eq. (43) (for hyperelastic membranes with surface tension). The unknown stretch k and the contact line position $\widetilde{R}_c$ are varied until the two boundary conditions at $\widetilde{R} = 1$ in Eq. (33) are satisfied. In practice, it is more convenient to vary Δ and k for a given $\widetilde{R}_c$ using the Newton method. For $J_m \to \infty$, Eq. (D.3) reduces to

$$\begin{aligned}
&\frac{\mathrm{d}}{\mathrm{d}\widetilde{R}}y_1 = \frac{y_4\cos y_3 - y_1}{\widetilde{R}},\\
&\frac{\mathrm{d}}{\mathrm{d}\widetilde{R}}y_2 = -y_4\sin y_3,\\
&\frac{\mathrm{d}}{\mathrm{d}\widetilde{R}}y_3 = -\frac{y_4\left(y_4^2y_1^4 - 1 + \mathcal{T}_s y_4^3y_1^3\right)\sin y_3/\widetilde{R} - \mathcal{P}y_4^4y_1^4}{y_1\left(y_4^4y_1^2 - 1 + \mathcal{T}_s y_4^3y_1^3\right)},\\
&\frac{\mathrm{d}}{\mathrm{d}\widetilde{R}}y_4 = \frac{y_4^2\left(y_4^2y_1^4 - 3\right)\cos y_3 - y_4y_1\left(y_4^4y_1^2 - 3\right)}{\widetilde{R}y_1\left(y_4^4y_1^2+3\right)},
\end{aligned} \tag{D.6}$$

which presents the equations for the neo-Hookean membranes.

Data availability

Data will be made available on request.

References

Akinwande, D., Brennan, C.J., Bunch, J.S., Egberts, P., Felts, J.R., Gao, H., Huang, R., Kim, J.-S., Li, T., Li, Y., et al., 2017. A review on mechanics and mechanical properties of 2D materials—Graphene and beyond. Extrem. Mech. Lett. 13, 42–77.

Andreotti, B., Snoeijer, J.H., 2020. Statics and dynamics of soft wetting. Annu. Rev. Fluid Mech. 52 (1), 285–308.

Argatov, I.I., 2021. Indentation mapping of stretched adhesive membranes. Proc. R. Soc. A Math. Phys. Eng. Sci. 477, 20210349.

Audoly, B., Pomeau, Y., 2000. Elasticity and geometry. In: Peyresq Lectures on Nonlinear Phenomena. World Scientific, pp. 1–35.

Barber, J., 2013. Similarity considerations in adhesive contact problems. Tribol. Int. 67, 51–53.

Barber, J.R., 2018. Contact Mechanics. Vol. 20, Springer.

Barber, J., Stupkiewicz, S., 2024. Indentation of a thin incompressible layer with finite friction. Int. J. Solids Struct. 298, 112868.

Begley, M.R., Collino, R.R., Israelachvili, J.N., McMeeking, R.M., 2013. Peeling of a tape with large deformations and frictional sliding. J. Mech. Phys. Solids. 61 (5), 1265–1279.

Bico, J., Reyssat, É., Roman, B., 2018. Elastocapillarity: when surface tension deforms elastic solids. Annu. Rev. Fluid Mech. 50 (1), 629–659.

Borodich, F.M., Galanov, B.A., 2016. Contact probing of stretched membranes and adhesive interactions: graphene and other two-dimensional materials. Proc. R. Soc. A Math. Phys. Eng. Sci. 472, 20160550.

Bradley, R.S., 1932. LXXIX. The cohesive force between solid surfaces and the surface energy of solids. Philos. Mag. J. Sci. 13 (86), 853–862.

Chen, E., Dai, Z., 2023. Axisymmetric peeling of thin elastic films: A perturbation solution. J. Appl. Mech. 90 (10).

Ciavarella, M., Joe, J., Papangelo, A., Barber, J.R., 2019. The role of adhesion in contact mechanics. J. R. Soc. Interface 16, 20180738.

Ciavarella, M., Zhang, S., Gao, H., Cricri, G., 2023. A linear cohesive model of zero degree peeling of a viscoelastic tape from a substrate. J. Adhes. Sci. Technol. 37 (12), 1906–1920.

Dai, Z., Hou, Y., Sanchez, D.A., Wang, G., Brennan, C.J., Zhang, Z., Liu, L., Lu, N., 2018. Interface-governed deformation of nanobubbles and nanotents formed by two-dimensional materials. Phys. Rev. Lett. 121 (26), 266101.

Dai, Z., Lu, N., 2021. Poking and bulging of suspended thin sheets: Slippage, instabilities, and metrology. J. Mech. Phys. Solids 149, 104320.

Dai, Z., Lu, N., Liechti, K.M., Huang, R., 2020. Mechanics at the interfaces of 2D materials: Challenges and opportunities. Curr. Opin. Solid State Mater. Sci. 24 (4), 100837.

Dai, Z., Rao, Y., Lu, N., 2022. Two-dimensional crystals on adhesive substrates subjected to uniform transverse pressure. Int. J. Solids Struct. 257, 111829.
Davidovitch, B., Vella, D., 2018. Partial wetting of thin solid sheets under tension. Soft Matter 14 (24), 4913–4934.
Eremeyev, V.A., Naumenko, K., 2015. A relationship between effective work of adhesion and peel force for thin hyperelastic films undergoing large deformation. Mech. Res. Commun. 69, 24–26.
Fang, Z., Dai, Z., Wang, B., Tian, Z., Yu, C., Chen, Q., Wei, X., 2022. Pull-to-peel of two-dimensional materials for the simultaneous determination of elasticity and adhesion. Nano Lett. 23 (2), 742–749.
Feng, D., Nguyen, A.V., 2017. Effect of contact angle and contact angle hysteresis on the floatability of spheres at the air-water interface. Adv. Colloid Interface Sci. 248, 69–84.
Freund, L.B., Suresh, S., 2004. Thin Film Materials: Stress, Defect Formation and Surface Evolution. Cambridge University Press.
Gennes, P.-G., Brochard-Wyart, F., Quéré, D., et al., 2004. Capillarity and Wetting Phenomena: Drops, Bubbles, Pearls, Waves. Springer.
GenRivlint, A.N., 1996. A new constitutive relation for rubber. Rubber Chem. Technol. 69, 59–61.
Goldsmith, N., 2016. The physical modeling legacy of Frei Otto. Int. J. Space Struct. 31 (1), 25–30.
He, L., Ding, K., 2009. Adhesive contact of a rigid sphere to finitely stretched substrates. Chin. Sci. Bull. 54 (11), 1970–1972.
Hu, J., Youssefian, S., Obayemi, J., Malatesta, K., Rahbar, N., Soboyejo, W., 2018. Investigation of adhesive interactions in the specific targeting of Triptorelin-conjugated PEG-coated magnetite nanoparticles to breast cancer cells. Acta Biomater. 71, 363–378.
Hui, C.-Y., Liu, T., Salez, T., Raphael, E., Jagota, A., 2015. Indentation of a rigid sphere into an elastic substrate with surface tension and adhesion. Proc. R. Soc. A Math. Phys. Eng. Sci. 471, 20140727.
Hutchinson, J.W., Suo, Z., 1991. Mixed mode cracking in layered materials. Adv. Appl. Mech. 29, 63–191.
Israelachvili, J.N., 2011. Intermolecular and Surface Forces. Academic Press.
Jensen, H., Thouless, M., 1993. Effects of residual stresses in the blister test. Int. J. Solids Struct. 30 (6), 779–795.
Johnson, K.L., Kendall, K., Roberts, A.D., Tabor, D., 1971. Surface energy and the contact of elastic solids. Proc. R. Soc. A Math. Phys. Eng. Sci. 324, 301–313.
Kendall, K., 1975. Thin-film peeling-the elastic term. J. Phys. D Appl. Phys. 8, 1449.
Khestanova, E., Guinea, F., Fumagalli, L., Geim, A., Grigorieva, I., 2016. Universal shape and pressure inside bubbles appearing in van der Waals heterostructures. Nat. Commun. 7 (1), 12587.
Kim, D.-H., Ghaffari, R., Lu, N., Rogers, J.A., 2012. Flexible and stretchable electronics for biointegrated devices. Annu. Rev. Biomed. Eng. 14 (1), 113–128.
Kitt, A.L., Qi, Z., Rémi, S., Park, H.S., Swan, A.K., Goldberg, B.B., 2013. How graphene slides: measurement and theory of strain-dependent frictional forces between graphene and SiO2. Nano Lett. 13 (6), 2605–2610.
Krieg, M., Fläschner, G., Alsteens, D., Gaub, B.M., Roos, W.H., Wuite, G.J., Gaub, H.E., Gerber, C., Dufrêne, Y.F., Müller, D.J., 2019. Atomic force microscopy-based mechanobiology. Nat. Rev. Phys. 1 (1), 41–57.
Laprade, E.J., Long, R., Pham, J.T., Lawrence, J., Emrick, T., Crosby, A.J., Hui, C.-Y., Shull, K.R., 2013. Large deformation and adhesive contact studies of axisymmetric membranes. Langmuir 29 (5), 1407–1419.
Li, H., Dai, Z., 2024. Adhesion of elastic microbeams on thin deformable substrates. Eng. Fract. Mech. 110634.
Li, H., Yu, C., Dai, Z., 2024. Regimes in the axisymmetric stiction of thin elastic plates. Int. J. Mech. Sci. 284, 109740.
Liu, T., Liu, Z., Jagota, A., Hui, C.-Y., 2020. Droplets on an elastic membrane: configurational energy balance and modified Young equation. J. Mech. Phys. Solids 138, 103902.
Long, R., Hui, C.-Y., 2012. Axisymmetric membrane in adhesive contact with rigid substrates: Analytical solutions under large deformation. Int. J. Solids Struct. 49 (3–4), 672–683.
Long, R., Shull, K.R., Hui, C.-Y., 2010. Large deformation adhesive contact mechanics of circular membranes with a flat rigid substrate. J. Mech. Phys. Solids 58 (9), 1225–1242.
Mansfield, E.H., 1989. The Bending and Stretching of Plates, second ed. Cambridge University Press.
Otto, F., 2015. Modeling with soap films. YouTube URL https://www.youtube.com/watch?v=-IW7o25NmeA.
Patil, A., DasGupta, A., Eriksson, A., 2015. Contact mechanics of a circular membrane inflated against a deformable substrate. Int. J. Solids Struct. 67, 250–262.
Patil, A., Nordmark, A., Eriksson, A., 2014. Free and constrained inflation of a pre-stretched cylindrical membrane. Proc. Math. Phys. Eng. Sci. 470 (2169), 20140282.
Paulsen, J.D., 2019. Wrapping liquids, solids, and gases in thin sheets. Annu. Rev. Condens. Matter Phys. 10 (1), 431–450.
Plaut, R.H., White, S.A., Dillard, D.A., 2003. Effect of work of adhesion on contact of a pressurized blister with a flat surface. Int. J. Adhes. Adhes. 23 (3), 207–214.
Rao, Y., Qiao, S., Dai, Z., Lu, N., 2021. Elastic wetting: Substrate-supported droplets confined by soft elastic membranes. J. Mech. Phys. Solids 151, 104399.
Rivlin, R., 1948. Large elastic deformations of isotropic materials. I. Fundamental concepts. Philos. Trans. R. Soc. A Math. Phys. Eng. Sci. 240 (822), 459–490.
Rivlin, R.S., 1997. The effective work of adhesion. In: Collected Papers of RS Rivlin: Volume I and II. Springer, pp. 2611–2614.
Ru, C., 2020. Adhesion of an elastic sphere on a tensioned membrane. Math. Mech. Solids 25 (8), 1534–1543.
Sanchez, D.A., Dai, Z., Wang, P., Cantu-Chavez, A., Brennan, C.J., Huang, R., Lu, N., 2018. Mechanics of spontaneously formed nanoblisters trapped by transferred 2D crystals. Proc. Natl. Acad. Sci. USA 115 (31), 7884–7889.
Scheludko, A., Nikolov, D., 1975. Measurement of surface tension by pulling a sphere from a liquid. Colloid Polym. Sci. 253, 396–403.
Schroll, R., Adda-Bedia, M., Cerda, E., Huang, J., Menon, N., Russell, T., Toga, K., Vella, D., Davidovitch, B., 2013. Capillary deformations of bendable films. Phys. Rev. Lett. 111 (1), 014301.
Shanahan, M.E., 2000. Adhesion of a punch to a thin membrane. C. R. Acad. Sci. Ser. IV Phys. 1 (4), 517–522.
Shi, J., Müftü, S., Wan, K.-T., 2011. Adhesion of an elastic convex shell onto a rigid plate. J. Adhes. 87 (6), 579–594.
Snoeijer, J.H., Andreotti, B., 2013. Moving contact lines: scales, regimes, and dynamical transitions. Annu. Rev. Fluid Mech. 45 (1), 269–292.
Srivastava, A., Hui, C.-Y., 2013. Large deformation contact mechanics of a pressurized long rectangular membrane. II. Adhesive contact. Proc. R. Soc. A Math. Phys. Eng. Sci. 469 (2160), 20130425.
Style, R.W., Jagota, A., Hui, C.-Y., Dufresne, E.R., 2017. Elastocapillarity: surface tension and the mechanics of soft solids. Annu. Rev. Condens. Matter Phys. 8 (1), 99–118.
Thouless, M., Jensen, H., 1992. Elastic fracture mechanics of the peel-test geometry. J. Adhes. 38 (3–4), 185–197.
Vella, D., 2019. Buffering by buckling as a route for elastic deformation. Nat. Rev. Phys. 1 (7), 425–436.
Wang, G., Dai, Z., Wang, Y., Tan, P., Liu, L., Xu, Z., Wei, Y., Huang, R., Zhang, Z., 2017. Measuring interlayer shear stress in bilayer graphene. Phys. Rev. Lett. 119 (3), 036101.
Williams, J., 1997. Energy release rates for the peeling of flexible membranes and the analysis of blister tests. Int. J. Fract. 87, 265–288.
Yang, F., 2011. Adhesive contact between a rigid axisymmetric indenter and a neo-hookean solid. J. Adhes. 87, 180–193.
Yang, X., Srivastava, A., Long, R., 2023. Adhesive contact of an inflated circular membrane with curved surfaces. Int. J. Solids Struct. 279, 112371.
Yi, X., Shi, X., Gao, H., 2011. Cellular uptake of elastic nanoparticles. Phys. Rev. Lett. 107 (9), 098101.
Yin, Y., Dang, R., Wu, D., Li, M., Li, Y., Gao, H., 2024. Mechanics of microblister tests in 2D materials accounting for frictional slippage. Carbon 229, 119495.
Yu, C., Zeng, W., Wang, B., Cui, X., Gao, Z., Yin, J., Liu, L., Wei, X., Wei, Y., Dai, Z., 2025. Stiffer is stickier: Adhesion in elastic nanofilms. Nano Lett. 25, 1876–1882.
Yuan, W., Ding, Y., Niu, X., Wang, G., 2024. Adhesion of a rigid sphere to a freestanding elastic membrane with pre-tension. J. Appl. Mech. 91.

Yuan, W., Wang, G., 2021. Adhesion between a rigid sphere and a stretched membrane using the dugdale model. Int. J. Solids Struct. 208–209, 214–220.
Yuk, H., Varela, C.E., Nabzdyk, C.S., Mao, X., Padera, R.F., Roche, E.T., Zhao, X., 2019. Dry double-sided tape for adhesion of wet tissues and devices. Nature 575 (7781), 169–174.
Zhang, K., Arroyo, M., 2017. Coexistence of wrinkles and blisters in supported graphene. Extrem. Mech. Lett. 14, 23–30.
Zheng, Y., Hu, Y., Cai, S., 2019. Contact mechanics of a gel under constrained swelling. J. Mech. Phys. Solids 124, 427–445.
Zhu, T., Li, G., Müftü, S., Wan, K.-t., 2017. Revisiting the constrained blister test to measure thin film adhesion. J. Appl. Mech. 84 (7), 071005.
Zhu, T., Müftü, S., Wan, K.-t., 2018. One-dimensional constrained blister test to measure thin film adhesion. J. Appl. Mech. 85 (5).
Zhu, Y., Ni, Y., Huang, C., Yu, J., Yao, H., Zheng, Z., 2024. Unified model for adhesive contact between solid surfaces at micro/nano-scale. J. Mech. Phys. Solids 196, 106004.